EXTERNAL CONTROL OF CANCER CELLULAR DYNAMICS USING ADAPTIVE MODEL PREDICTIVE CONTROL

Benjamin Smart[1], Irene de Cesare[2], Ludovic Renson[1], Lucia Marucci[2,3,4]

[1]Department of Mechanical Engineering, Imperial College London, London SW7 1AY, U.K.

[2]Department of Engineering Mathematics, University of Bristol, Woodland Road, Bristol BS8 1UB, U.K.

[3]BrisSynBio, Life Sciences Building, University of Bristol, Tyndall Avenue, Bristol BS8 1TQ, U.K.

[4]School of Cellular and Molecular Medicine, University of Bristol, University Walk, Bristol BS8 1TD, U.K.

e-mail: b.smart21@imperial.ac.uk

Abstract

Recent advancements in Cybergenetics have lead to the development of new computational/experimental platforms that enable to robustly steer cellular dynamics by applying external feedback control. Such technologies have never been applied to regulate intracellular dynamics of cancer cells. Here, we show *in silico* that Adaptive Model Predictive Control (MPC) can effectively be used to steer signalling dynamics in Non-Small Cell Lung Cancer (NSCLC) cells to resemble those of wild-type cells, and to support the design of combination therapies. Our optimization-based control algorithm enables tailoring the cost function to force the controller to alternate different drugs and/or reduce drug exposure to minimize both drug-induced toxicity and the possibility to cause resistance to treatment. Our results pave the way for new cybergenetics experiments in cancer cells for drug combination therapy design.

keywords

Adaptive Model Predictive Control (MPC), Combination Therapies, Cybergenetics, External Feedback Control, Non-Small Cell Lung Cancer (NSCLC)

1 Introduction

Cybergenetics is a recent field of synthetic biology, which refers to the forward engineering of complex phenotypes in living cells applying principles and techniques from control engineering [1].

Three main approaches have been proven to be effective for the control of different processes (e.g. gene expression, cell proliferation) in living cells, namely: i) open- or closed-loop controllers embedded into cells by means of synthetic gene networks [2–6]; ii) external controllers, where the controlled processes are within cells, while the controller (either at single or cell-population level) and the actuation functions are implemented externally via microfluidics-optogenetics/microscopy-flow cytometry platforms and adequate algorithms for online cell output quantification and control [7–16]; iii) multicellular control, where both the control and actuation functions are embedded into cellular consortia [17–20].

Plenty of examples of embedded controllers have been engineered across different cellular chassis; instead, applications of external and multicellular controllers in mammalian cells are scarce and either just theoretical or limited to proof of concepts.

Here, we propose to apply cybergenetics, in particular external feedback control, to predict combinations of drugs (i.e. control inputs) which can bring dysregulated cellular variables (i.e. gene expression, control output of the system) within tightly controlled ranges in cancer cells.

We take Non-Small Cell Lung Cancer as an example and we use a previously proposed differential equations mathematical model describing the dynamics of the EGFR and IGF1R pathways to show, in silico, that external feedback controllers can effectively steer intracellular gene expression dynamics in cancer cells to resemble those of wild-type cells.

The use of feedback control is advantageous as it enables coping with changes in both steady-state levels and in the temporal dynamics of genes involved in dysregulated signalling cascades. The control action is implemented by means of an Adaptive Model Predictive Controller (MPC), thus not requiring a known model of the system; this is particularly advantageous in biological applications, where the derivation of detailed models can be time-consuming and troublesome [21–23].

The possibility to control single/multiple outputs with one or more inputs can support the design of combination therapies which target different nodes in signalling cascades; this approach can be advantageous to maximise the efficacy of cancer therapies [24]. In this regard, our optimization-based control algorithm enables tailoring the cost function to force the controller to alternate different drugs and/or reduce drug exposure; this approach can be beneficial to minimize both drug-induced toxicity and the possibility to cause resistance to treatment.

The controller should also be able to cope with the crosstalk among different signalling pathways and the presence of endogenous feedback loops within signalling pathways, which might be a further mechanism causing resistance by adaptive cellular responses in cancer cells [25].

In what follows, we ... .

2 Method

The model of a NSCLC system developed in [26] including the mTOR and MAPK pathways and some of the reactions between the two pathways, as shown in Figure 1. This model compares the affect of NSCLC cell with an EGF and IGF receptor over-expression in comparison to a wild type cell (i.e. a cell without cancer). An external feedback loop is needed to control the NSCLC system. Figure 1 shows the two outputs and three inputs used. The inputs I_1 to I_3, target 3 specific proteins within the pathways shown, preventing the molecules activation. The method and results within this project are entirely computational, but the inputs/outputs have been chosen such that the controller can be used for *in-vitro* experiments in the future. The pathways do not coexist independently within the cytoplasm, there are multiple reactions creating feedback loops between the pathways, which will be referred to as crosstalk.

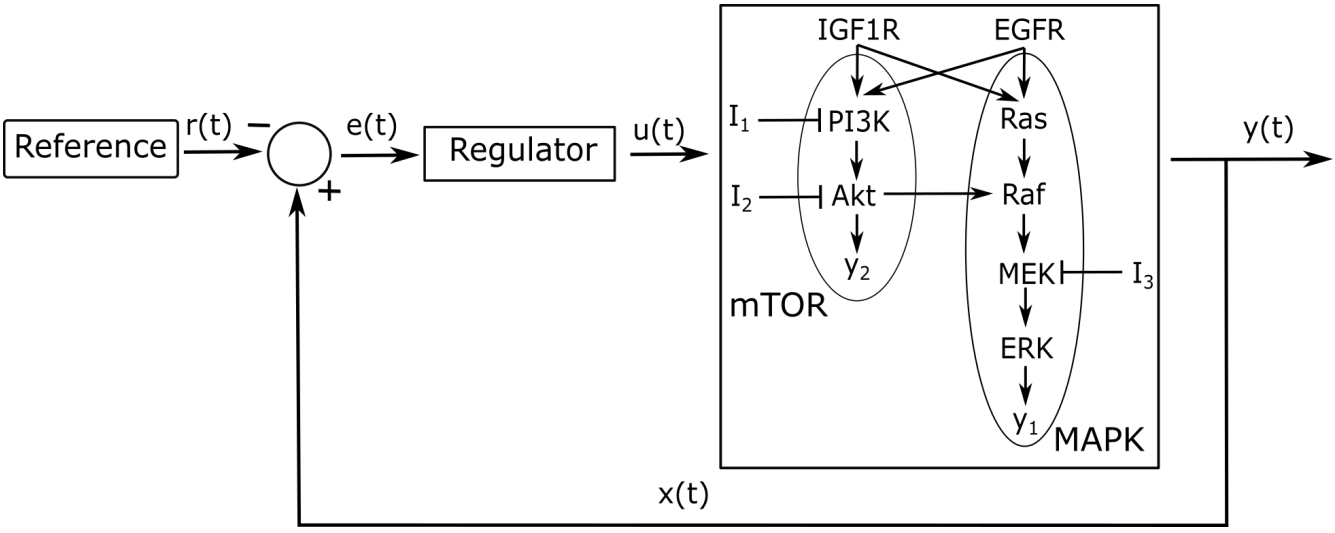

Figure 1: A control scheme including three inputs, (I_1 to I_3), that interact with the mTOR and MAPK pathways. Two observable protein concentrations, Akt and ERK, are recorded as outputs to the two pathways (y1 and y2). The regulator used throughout this project is an adaptive MPC program which will attempt to steer the concentrations of Akt and ERK to the transient response of the wild type cell, as set by the reference, as shown in Figure 2

Figure 2 shows the difference between the wild type cell and the NSCLC patient for each of the outputs, y1 (Akt) and y2 (ERK), in Figure 1. The term 'Free', refers to a free response of the NSCLC system with no inputs added. It can be seen that the over-expression of EGFR and IGFR causes a significant increase in the peak and duration of the activation in both y1(ERK) and y2(Akt). It should be noted that the activation of y1(ERK) occurs over a timescale of an order of magnitude faster than the activation of y2(Akt).

2.1 Controller

The two pathways shown in Figure 1 are both kinase activated cascades, meaning that an activation at the receptors in the cell membrane causes a cascade of phosphorylation that we see as activations in the internal states. The outputs that can be measured are nearer the end of each pathway, whilst the inputs act on molecules higher in the

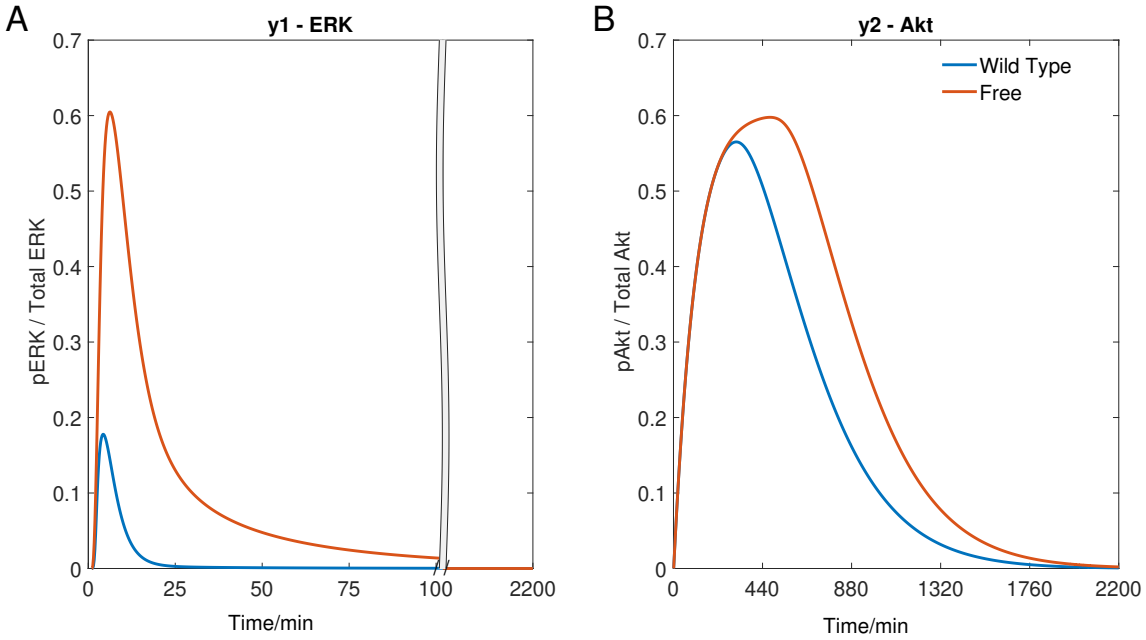

Figure 2: Simulations of the NSCLC model compared to a normal patient. The Wild type response is taken from [26] and the Free response is taken from the same paper but simulated with an over-expression of EGFR and IGFR. A) The response of ERK to an activation. B) The response of Akt to an activation. A wild type activation is caused by an active concentration of 8000 μM for both EGFR and IGFR and a NSCLC activation is triggered by an active concentration of 800'000 and 400'000 μM for EGFR and IGFR respectively.

cascade. Therefore it is difficult to robustly control the system as once an error is measured in the outputs, it is too late to have a significant affect by acting on the internal states higher up the cascade.

A model based controller is needed to interpret a small change in the outputs, rather than using a model free controller with a large gain that will have a large reaction to all errors in the outputs. For example a PID controller can be tuned such that the reaction to the initial error of the outputs is enough to mimic the reference, however the response is so finely tuned that robust control is not achieved (Section S6). A controller that can preempt the activation curve in the outputs by estimating the changes in internal states higher up the cascade will have better control of the NSCLC system.

A model based controller using adaptive MPC is used in this project, shown as the Regulator block in Figure 1, using a given mathematical model to predict the future behaviour of the system and act according to the minimum of a defined cost function, as described in Section S3. The success of MPC relies on the quality of the model used in the controller and the cost function in which the controller is using to calculate the 'optimum'. The novelty of this project lies in the choice of adaptive model and cost function.

2.1.1 MPC Model

The NSCLC model [26], contains significant non-linear dynamic terms as well as a large number of internal states therefore an adaptive MPC controller which computes a linear approximation of the NSCLC model at each time

step of the controller is used to predict the future of the internal states. The controller then applies the first input of its calculated 'optimal' input profile. At the next time step the controller recalculates a new linear model by linearising the NSCLC model. The use of a linear system results in a convex optimisation problem which the controller can quickly solve. An Adaptive MPC controller is used in all simulations unless stated otherwise.

Alternatively a non-linear MPC controller could have be used but it is very computationally heavy and could take longer to compute the next input to the system than the actual time step between inputs, as discussed in Section S5. The non-linear MPC performs slightly better than the linear Adaptive MPC, however it takes 2700 times longer to run the program.

2.1.2 Cost Function

$$J(\mathbf{U}) = \left(\mathbf{U}^T\mathbf{H}(\alpha,\beta,\gamma)\mathbf{U} + 2\mathbf{e}_0^T\mathbf{F}(\alpha,\beta,\gamma)\mathbf{U}\right) + \left(\mathbf{U}^T\tilde{\mathbf{P}}(\eta)\mathbf{U} + \tilde{\mathbf{p}}(\eta)\mathbf{U}\right) + \left(\mathbf{U}^T\mathbf{D}(\theta)\mathbf{U} + \mathbf{d}(\theta)\mathbf{U}\right) \quad (1)$$

The cost function, $J(\mathbf{U})$, used in the simulations, (derived in Section S3) is dependent on only the current state of the error signal, $\mathbf{e}_0$, and the inputs used, $\mathbf{U}$.

The standard cost function used for a linear MPC controller is explained in [27] and derived in Section S3.1.1, containing the first two terms of Equation (1). Using $\mathbf{H}$ and $\mathbf{F}$ to focus on the proportion error in the states, $\mathbf{e}$, and the input concentrations, $\mathbf{u}$.

It has been shown that to reduce the downstream affect of a mutation it is not only beneficial to reduce the peak of the output but also its duration [28]. Therefore, an output with a relatively small error for a long time can have a similar downstream effect to an output with a short error with a large amplitude. In order to cost both the magnitude and duration of the state error, $\mathbf{e}$, an integral term is added to the cost function in addition to the standard cost function, as shown in the third and forth term of Equation (1), using matrices $\tilde{\mathbf{P}}$ and $\tilde{\mathbf{p}}$. These matrices are derived in Section S3.3. Costing the integral of the state errors rather than the direct error will cause the controller to focus more on the inputs higher up the cascade as these have more of an effect on the duration of the outputs rather than just the peak [28].

It had been found that there were sections of the simulations where the inputs fluctuated rapidly between the upper and lower bounds of the allowed inputs ($\mathbf{U}_L = 0\mu M$ and $\mathbf{U}_U = 1\mu M$). This rate of change of the input is not optimal, therefore it would better represent the 'optimal' input if the cost function could also include the rate of change of the input. A differential cost of the inputs is also added to $J(\mathbf{U})$ in the fifth and sixth terms of Equation (1), using matrices $\mathbf{D}$ and $\mathbf{d}$. $\mathbf{D}$ and $\mathbf{d}$ are derived in Section S3.2.

The focus of the cost function is decided by varying the weights of term coefficients $(\alpha, \beta, \gamma, \eta, \theta)$ to tell the controller what an optimum solution favours.

The MPC simulations are reproducible due to the deterministic nature of the model and controller, as long as the cost function coefficient weights and other MPC related parameters are consistent. Therefore several key parameters are added to the caption of each figure. Table 1 gives a summary of these parameters.

Parameter	Description	Example Value
T_s	Sample time of the MPC regulator - duration between when the MPC regulator is initiated and the future inputs predicted.	1min
N	The length of the prediction horizon - the number of steps into the future that the MPC will predict the states and optimum input.	10 steps
α	The weight of the internal state errors.	0.01
β	The extra weight associated with the output state errors.	1
γ	The weight of the input profile, a row vector for each of the inputs, I_1 to I_3 respectively.	[1 1 1]
θ	The weight of the gradient of the input profile.	0.5
η	The weight of integral of the internal state errors.	1

Table 1: The Parameters used for each MPC simulation

2.1.3 Indexes

To assess quantitatively the performance of our controller, we define an Error Index, EI, is the sum of the squared error between the output and the reference for the outputs, as used in [29].

$$EI = \int_0^T \mathbf{e}^T \mathbf{C} \mathbf{e} \, dt \tag{2}$$

The matrix $\mathbf{C}$ is the output matrix of the linearised NSCLC model. This index is displayed in the top left corner of the output plots. The smaller the EI the smaller the integral squared error and therefore the outputs are closer to the references.

To get a sense of the controller effort needed to achieve a certain output, we assess the dose of input drug receive by the cell using a Dose Index, DI_i. It is the integral of the input signal, where $\mathbf{u}(t) = [I_1(t), I_2(t), I_3(t)]$.

$$DI_i = \int_0^T I_i(t) \, dt \tag{3}$$

It can be seen on the right of each individual input plot. The inputs can never be negative as they are a physical concentration, therefore there is no need to square the input signal.

3 Result

Non-Small Cell Lung Cancer (NSCLC) accounts for 80% of lung cancer cases and is characterised by various mutation which usually lead to an over expression of the EGF and IGF receptors, embedded in the cell membrane. These receptors trigger several cascades including the mTOR and MAPK pathways, as shown in Figure 1. The mTOR

pathway produces the protein FOXO1, which helps to control the process of Apoptosis (planned cell death), whilst the MAPK pathway produces C-FOS which regulates cell proliferation, which can both lead to the development of tumours if not properly regulated. ERK and Akt, noted as $y1$ and $y2$ respectively, are the proteins that can be produced alongside a fluorescent marker, such that the concentration can be observed from outside the cell and have therefore been chosen as the outputs.

3.1 Assessing the Importance of Each Term in the Cost Function

Firstly Single Input Single Output (SISO) simulations were performed. The controller tries to steer the dynamics of either y1(ERK) or y2(Akt) by varying the concentrations of the drug that acts directly on the outputs pathway (I_3 for y1(ERK) and either I_1 or I_2 for y2(Akt)). Figure 3 uses I_2 to act on y2(Akt) to compare the affect of each pair of terms in Equation (1) on the performance of the controller.

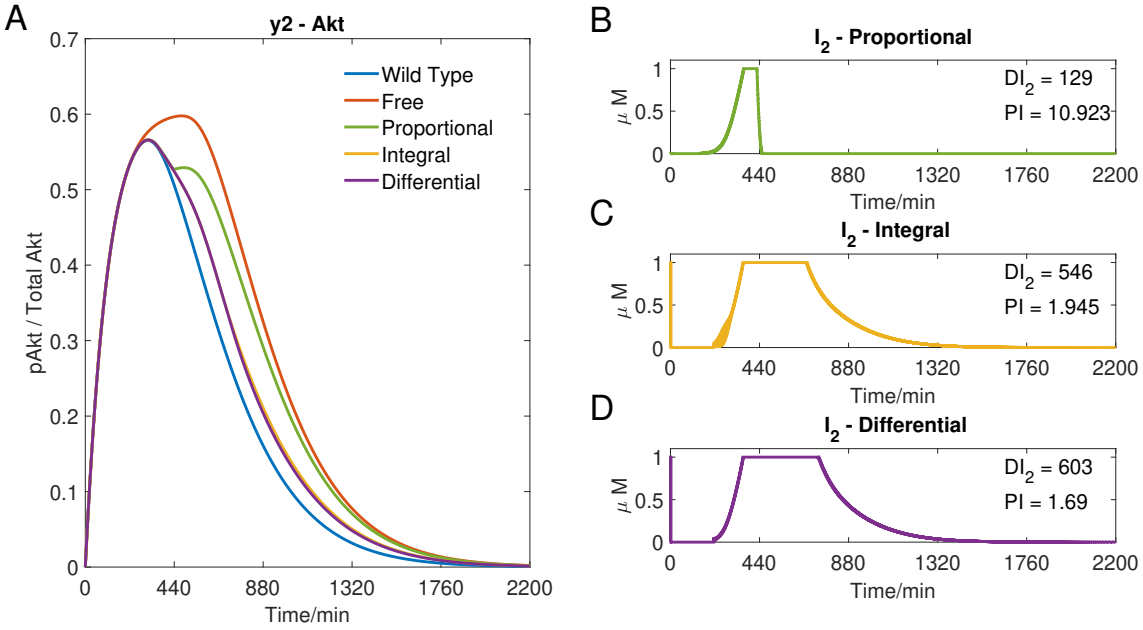

Figure 3: Single-Input Single-Output (SISO) Linear MPC simulation using I_2 to control y2 - Akt comparing the affect of the integral error and a differential of the inputs to the cost function in Equation (1). A) The response of y2(Akt) to the respective inputs. B) The input profile of I_2 using the proportional error within the cost function (matrix H and F of (1)). Parameters: $\alpha = 0$, $\beta = 1$, $\gamma = [-, 10^5, -]$, $\theta = 0$ and $\eta = 0$. C) The input profile of I_2 using the integral error within the cost function (using only the $\tilde{P}$ and $\tilde{p}$ terms of (1)). Parameters: $\alpha = 0$, $\beta = 0$, $\gamma = [-, 10^5, -]$, $\theta = 0$ and $\eta = 1$. D) The input profile of I_2 using the integral error and a differential cost on the inputs within the cost function (matrices $\tilde{P}$, $\tilde{p}$, D and d in (1)). Parameters: $\alpha = 0$, $\beta = 0$, $\gamma = [-, 10^5, -]$, $\theta = 10^5$ and $\eta = 1$. $T_s = 1min$ and $N = 10$ for all plots.

Figure 3 shows that using an integral term within the MPC cost function reduces the overall error in a cellular cascade system. It can be seen in plots A) that the MPC controller including the integral ~ (and integral with differential ~) cost has a far smaller error when compared to the proportional ~ cost. The integral cost simulation ~ has an Error Index five times lower than the simulation based on the proportional error ~.

However it can be seen in plot C) there is a section of the input that looks like a solid block where the input is fluctuating each time step (between 250-300 minutes). Plot D) show that the gradient cost causes the fluctuations of the input to decrease significantly. Plot D) also shows the lowest Error Index of the three simulations – but the highest Dose Index. This is due to the fact that the cost function weightings are all relative to each other, therefore including the differential term in the cost function means that the input term is less important and therefore the controller uses more of the input, and subsequently achieves a lower Error Index at the cost of a higher Dose Index.

The derivative term is kept here to show the versatility of the controller but is not included in further simulations in order to simplify the tuning of combinational therapies when the figures show the balance between the Error and Dose Indexes. As previously discussed, including the differential term can have adverse affects in changing the Dose Index without changing the input weights and is therefore not included in subsequent figures. Apart from the weight associated with each input the weight of each term in the subsequent cost functions is consistent with plot C).

3.2 Single-Input Single-Output Control

Through using feedback control the NSCLC cells can appear like wild type cells and therefore the aim of the simulations is to get the closed loop response to follow the wild type response such that anything downstream of the cascade will respond in the same way as the wild type cell. In order to show that using a combination of the three different inputs is better than using any one of the inputs, the 'optimal' input for each one of the input is simulated. Figure 4 shows Single-Input Single-Output (SISO) MPC simulations for I_1, I_2 and I_3. The output for each plot is in the same signalling pathway as the target in which the drug acts upon, as shown in Figure 1. It can be seen that plots C) and D) of Figure 4 are identical to parts of plot A) and plot C) of Figure 3 as these are both SISO responses of I_2 using the chosen cost function (an integral cost function). It can be seen that all of the SISO responses move the NSCLC patient towards the reference using a lower dose than just a step of each input at the maximum allowed dose, decreasing both the Error and Dose Indexes. Therefore demonstrating the benefits of even using a simpler SISO control scheme within an external feedback loop as compared to the standard treatment of a static step input.

3.3 Multi-Input Multi-Output Control

The same controller can be used to steer both outputs using all three inputs, in a Multi-Input Multi-Output (MIMO) simulation, as shown in Figure 5. It can be seen that error of y2(Akt) (Figure 5B) is significantly smaller in comparison to Figure 4A and C, whilst using significantly less of I_1 and I_2. As can be seen in the reduction of the Error Index for y2(Akt) ($0.791 < 1.954 < 2.75$) and the reduction in the Dose Index for each input ($570 < 1068$ and $418 < 546$). Hence showing the benefit of using adaptive MPC to produce drug profiles for combination therapies.

However, due to the speed of the MAPK pathway compared with the MIMO controller, the output y1(ERK)

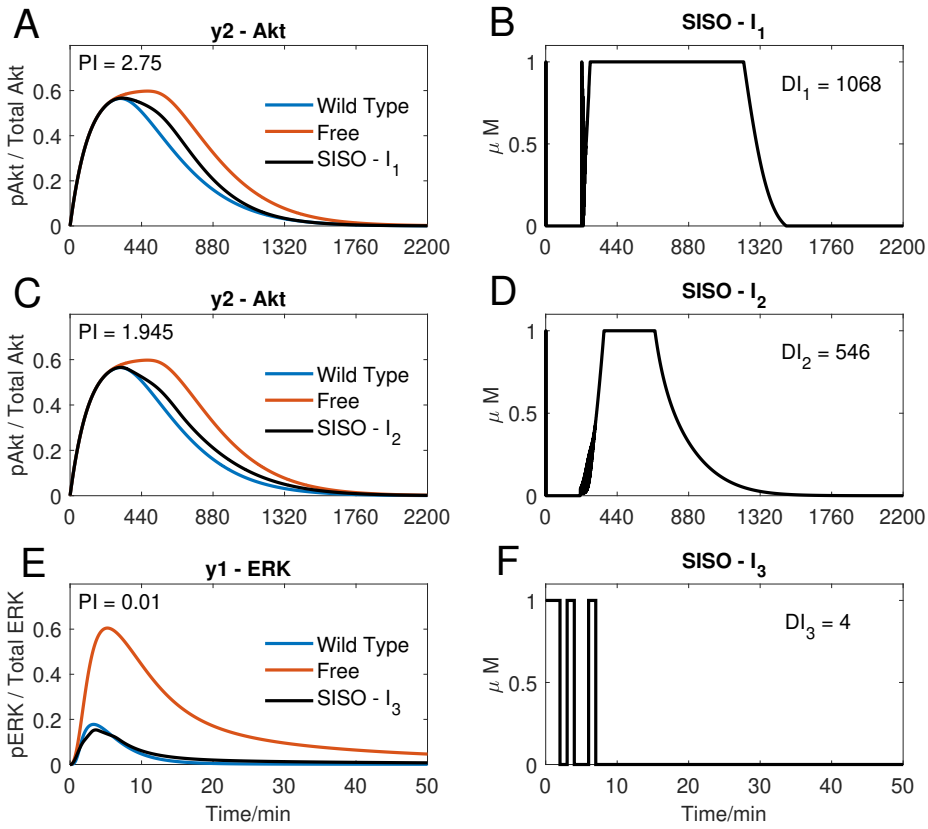

Figure 4: SISO Linear MPC simulations. A) The response of Akt to the input of I_1 in plot B). B) The input profile of I_1. Plots A) and B) used the input weights $\gamma = [1, -, -]$. C) The response of Akt to the input of I_2 in plot D). D) The input profile of I_2. Plots C) and D) used the input weights $\gamma = [-, 10^5, -]$. E) The response of ERK to the input in plot F). F) The input profile of I_3. Plots E) and F) used the input weights $\gamma = [-, -, 10^9]$. Parameters in plots A)-f): $T_s = 1$, $N = 10$, $\alpha = 0$, $\beta = 0$, $\theta = 0$ and $\eta = 1$.

fails to adequately follow the reference activation curve (causing the large EI in Figure 5A). Figure 6 shows that if the time step is adequately reduced (for instance, to 0.02 minutes), the controller can handle the faster dynamics of the pathway and effectively control both outputs whilst using a lower dosage of all the inputs and therefore potentially a less toxic drug profile.

3.4 Combinational Therapies

As a NSCLC cell is currently given one inhibitor for an extended period of time, it could experience severe side affects from the high dose and become resistant to the inhibitor over time [24], therefore the controller should be used to find potential drug profiles that can achieve a similar Error Index (EI) whilst varying the dose of the inputs (DI). The weight associated with using each input, γ, within the cost function can be varied in order to decide how readily the controller uses each input, therefore these weights can be varied between simulations to achieve a small EI whilst using different doses of each drug, as shown in Figure 7. The formation of the normalised Error

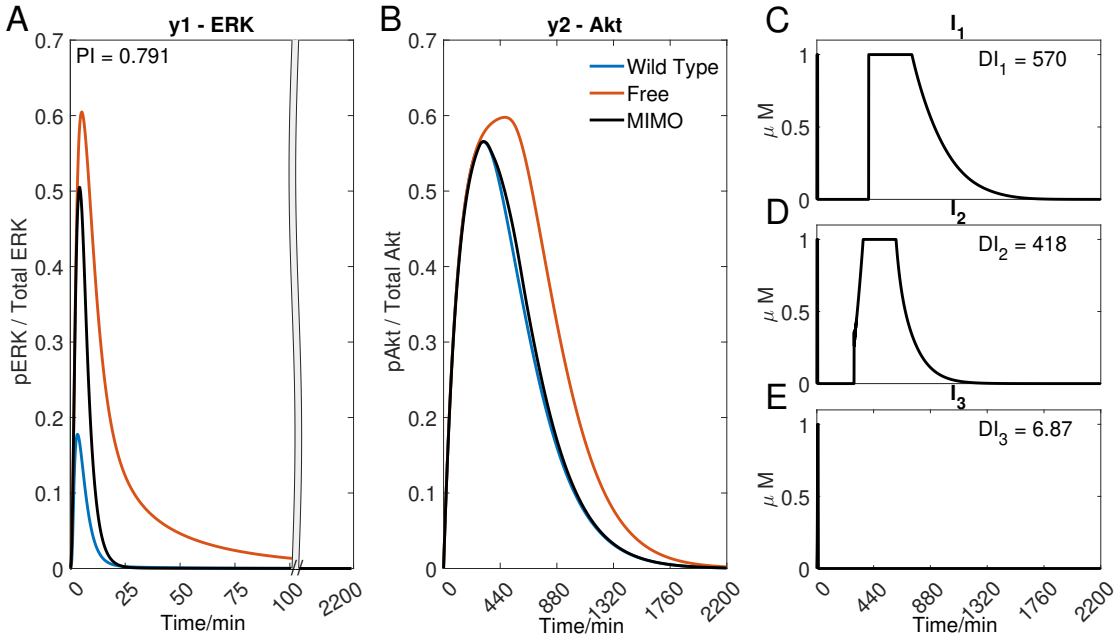

Figure 5: A MIMO Linear MPC simulation using I_1, I_2 and I_3 to control the concentration of y1 - ERK and y2 - Akt. A) The response of ERK. B) The response of Akt. C) to E) The inputs used in the simulation. Parameters: $T_s = 1min$, $N = 10$, $\alpha = 0$, $\beta = 0$, $\gamma = [1, 10^5, 10^9]$, $\theta = 0$ and $\eta = 1$.

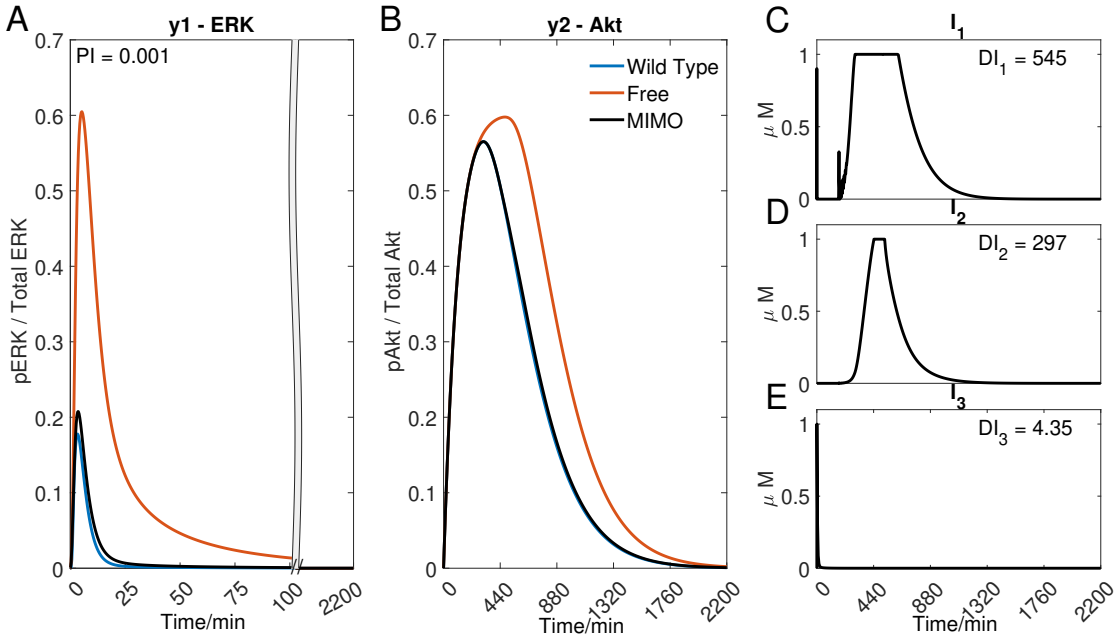

Figure 6: A MIMO Linear MPC simulation using I_1, I_2 and I_3 to control the concentration of y1 - ERK and y2 - Akt. A) The response of ERK. B) The response of Akt. C) to E) The inputs used in the simulation. Parameters: $T_s = 0.02min$, $N = 10$, $\alpha = 0$, $\beta = 0$, $\gamma = [1, 10^5, 10^9]$, $\theta = 0$ and $\eta = 1$.

Index and Dose Index is shown in the Supplementary Information, Equations (S40) and (S41), respectively. The Bliss Independence (BI) formula [30, 31], has been used as a combined normalised Dose Index and is discussed in Section S4 of the supplementary Information. BI is used to summarise the combined effect of the drugs used in the

combination therapy.

Figure 7 focuses on the control of y2 (Akt), which can only be affected by I_1 and I_2. The weight associated with the two inputs can be varied as a ratio of $R = \frac{\gamma_2}{\gamma_1}$ ranging from a high weight associated with I_1, γ_1, producing a SISO plot only using I_2 all the way through to a high R value, where γ_2 is relatively large and the controller will only choose to use I_1, as shown. The figure compares the Error Index, EI, and the Bliss Independence, BI, to the weight ratio, R. Showing there is a range of ratios where both inputs are used, significantly reducing EI and therefore improving the performance of the controller, whilst reducing BI. Therefore the performance of the MISO controller is better than any SISO simulation, whilst also being less toxic. The 'optimum' input has been defined as the location where the performance of the controller is 'optimal', and therefore the minimum of EI.

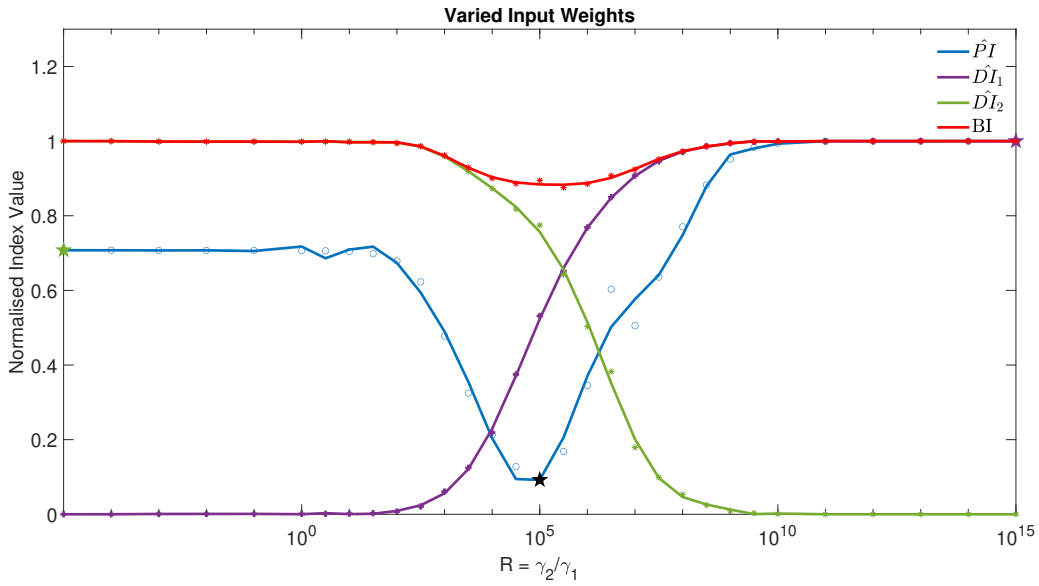

Figure 7: The normalised Error Index and normalised Dose Index recorded from different MISO linear MPC simulations using I_1 and I_2 to control the concentration of y2 - Akt. A line of best fit has been used to fit the markers taken from different MISO MPC simulations. The plot shows EI and DI for varied ratio of weights between γ_2/γ_1, for example, when $R = 100$, $\gamma = [1, 100]$ Parameters: $T_s = 1min$, $N = 10$, $\alpha = 0$, $\beta = 0$, $\theta = 0$ and $\eta = 1$. The three star markers show the ratio used in the plots of Figure 8

It can be seen from Figure 7 that the minimum occurs when $R = 10^5$, corresponding to $\gamma_1 = 1$ and $\gamma_2 = 10^5$. The Multi-input Single-Output (MISO) simulation at that optimum is compared to the responses at a very low R value and very high R value in Figure 8. It can be seen that not only is the Error Index significantly lower (0.25 as oppose to 2.75 and 1.95 in Figure 4 A) and C) for I_1 and I_2 respectively) but the simulation also uses less of each drug to achieve this ($568 < 1068$ for I_1 and $423 < 546$ for I_2), showing the benefits of using adaptive MPC to effectively tune the response of the control system to find different combinational therapies which perform similarly well (and all better than a step input of one drug).

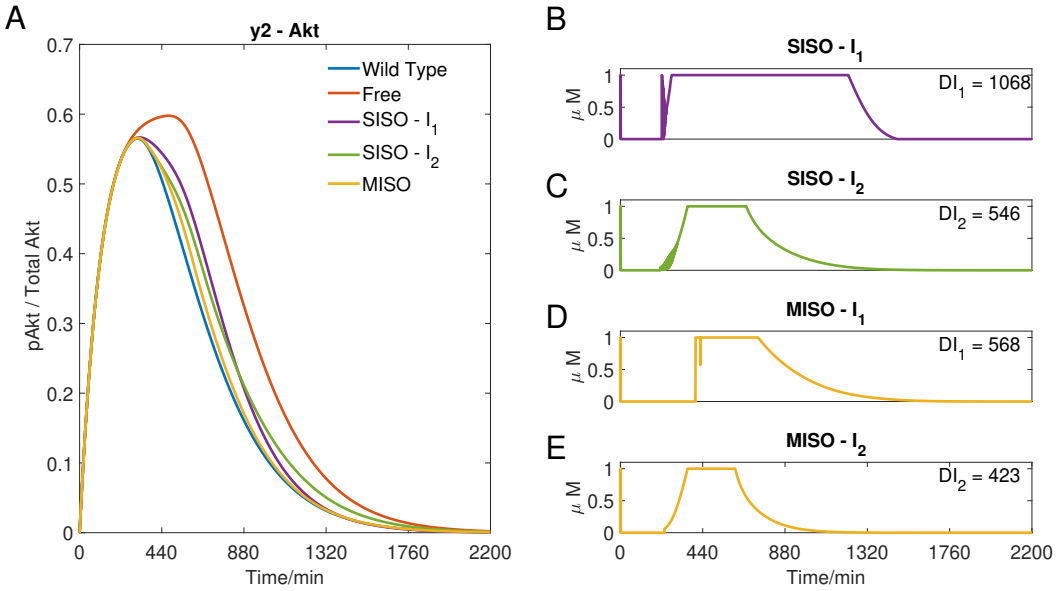

Figure 8: Three Linear MPC simulation using I_1 and I_2 to control the concentration of y2 - Akt. A) the response of Akt to three different input weightings, SISO - I_1 where $\gamma = [1, 10^{15}]$, SISO - I_2 where $\gamma = [1, 10^{-5}]$ and MISO, where $\gamma = [1, 10^{5}]$. The MISO γ was selected from the minimum point of Figure 7 of the Error Index, EI. B) the input of I_1 used in the SISO simulation, resulting in $EI = 2.7495$. C) the input of I_2 used in the SISO simulation, resulting in $EI = 1.9454$. D) and E), the inputs of I_1 and I_2, respectively, used in the MISO simulation, resulting in $EI = 0.25341$. The other weightings of the cost function described and other MPC constants: $T_s = 1min$, $N = 10$, $\alpha = 0$, $\beta = 0$, $\theta = 0$ and $\eta = 1$

3.5 Drug Holidays

The controller can be used with predefined segments where the controller gives the cell a break from one drug to give the patient a break from one of the drugs in order to slow the process of growing resistance to the inputs whilst still achieve a similar EI. These Drug Holidays can be achieved by varying the weights associated with each input within the cost function during the simulations. Figure 9 shows that the controller can retain a similarly low Error Index whilst swapping inputs after 600 minutes. Therefore it is shown that a programmed change of cost function weights during the simulation can decide when each input should be used.

Instead of choosing times when each drug can be used the controller can also be set to only be able to choose one of the inputs at each point in time. The inputs shown in Figure 10 have an ON or OFF state, $1\mu M$ or $0\mu M$. The step size used makes a large difference to the response as when $T_s = 1min$ the inputs rapidly fluctuate but a discrete MISO simulation where have larger regions where the inputs alternate, however the simulations achieves a relatively good EI ($1.46 < 2.75$ and 1.95) using less inputs than either SISO response ($634 < 1068$ and $447 < 546$). However flicking the inputs ON and OFF every minute might be tricky, therefore a longer time step can be used. Figure 10 shows the discrete simulation when $T_s = 30min$, it can be seen that the inputs can only be changed every half an hour so there is not the same regions where the inputs are flicking ON and OFF. It can also be seen that there is a better EI as $1.6878 < 2.75$, whilst still using less of each input than the SISO responses ($630 < 1068$ and $450 < 546$).

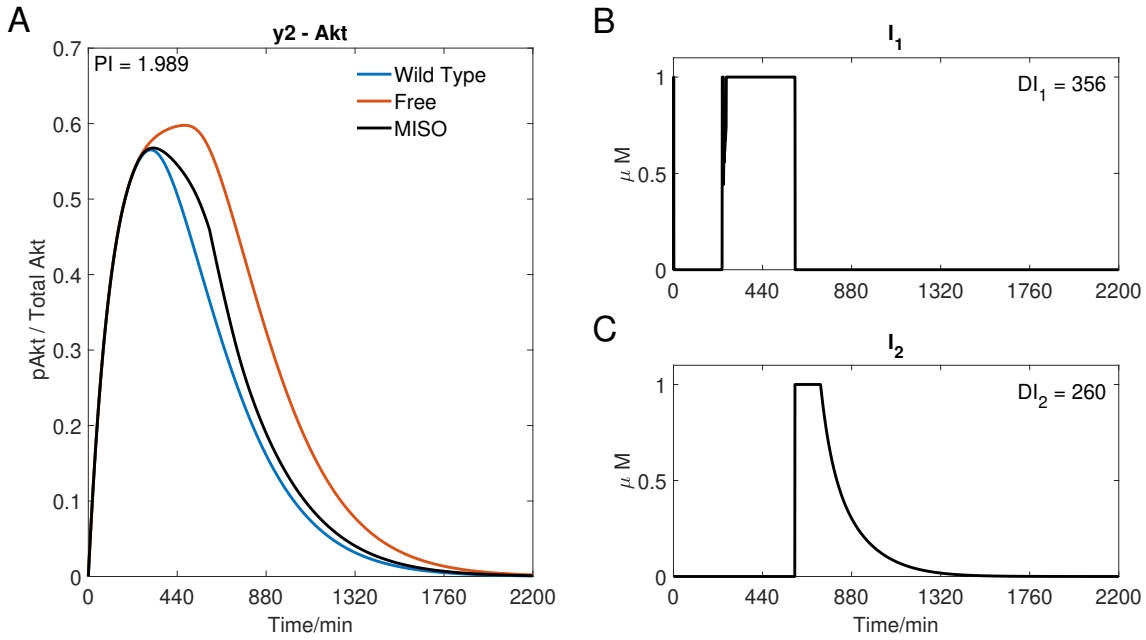

Figure 9: Swapping between which drugs are administered. A MISO Linear MPC simulation using I_1, I_2 to control the concentration of y2 - Akt. A) The response of Akt. B) to C) The inputs used in the simulation. Parameters: $T_s = 1min$, $N = 10$, $\alpha = 0$, $\beta = 0$, $\gamma = [1, \infty, -]$ when $0 \leq t \leq 600min$ and $\gamma = [\infty, 10^5, -]$ when $600 < t \leq 2200min$, $\theta = 0$ and $\eta = 1$.

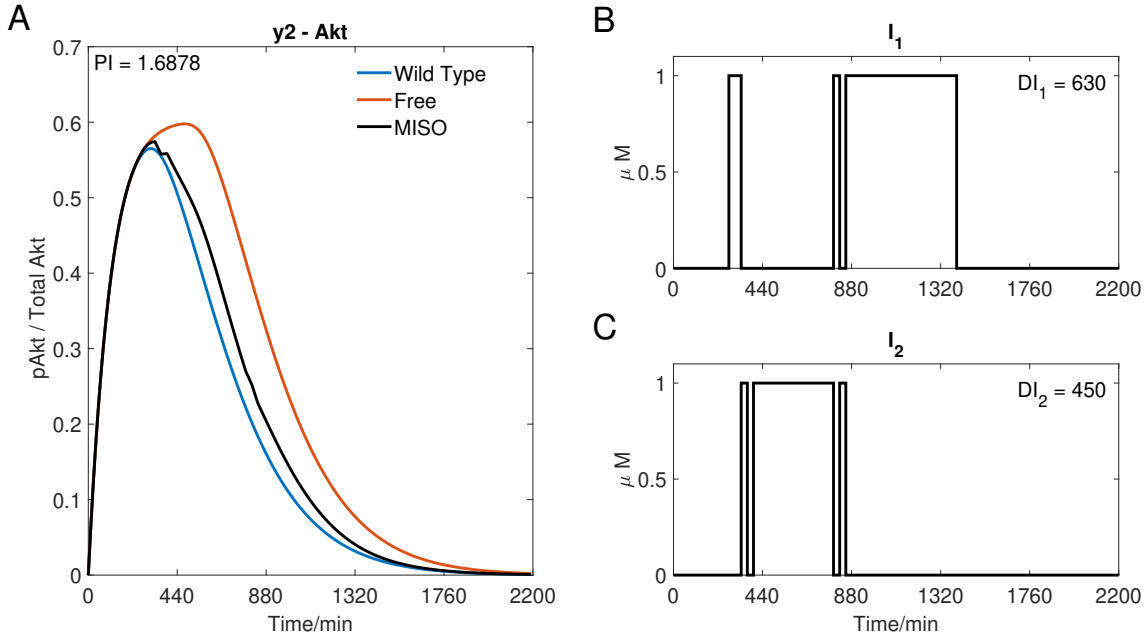

Figure 10: A discrete MISO Linear MPC simulation using I_1 and I_2 to control the concentration of y2 - Akt. A) The response of Akt. B) and C) The inputs used in the simulation. Parameters: $T_s = 30min$, $N = 10$, $\alpha = 0$, $\beta = 0$, $\gamma = [1, 10^5, -]$, $\theta = 0$ and $\eta = 1$.

4 Discussion

Computational methods have been extensively used in the search for effective cancer treatments, with approaches including optimal control to regulate dynamics of different cell populations, possibly accounting for competition mechanisms [1,2,7,10,16,32–36], and a feedback action to account for changes in the cancer system, either in-silico or in-vivo, to act in real time [9,11,29,37]. This is, to the best of our knowledge, the first attempt of using feedback control to regulate intracellular dynamics in cancer cells.

We showed that an adaptive MPC program can be used to inform treatments for NSCLC cells, steering the dynamics of several key signalling pathways, whilst offering a tunable cost function that allows to adjust the characteristics of an 'optimal' input. The controller can be tuned to choose different drug profiles that will achieve a similar control performance whilst reducing exposure to one or more drugs.

Other control strategies, like PID controllers, are less straight forward to tune as the gains are not so related to the observed output and desired input. The use of a linear model within the MPC algorithm makes the control algorithm running time short enough for it to be used, in the future, in external feedback control experiments. The implementation of those would require some practical aspects to be considered, which we did not account for. Firstly, there might be delays in cell responses to drugs/actuation, which the model used by the controller should account for. Also, the sampling/actuation time might need to be fast enough, if aiming at controlling genes with fast dynamics. This issue might be overcome using experimental optogenetics-based platforms instead of microfluidics-based ones, as they can reduce delays in the actuation.

We foresee a growing interest in applying cybergenetics approaches, and in particular feedback controllers, to steer mammalian cells dynamics. If we realize our ambition to implement the experiments proposed here on living cells and, longer term, on patient-derived organoids, feedback control might be a valuable tool for the design or personalized optimal treatments for a range of conditions.

5 Conclusion

It has been demonstrated that an adaptive MPC program can be used to better inform treatments for a NSCLC cell, guiding the behaviour of several key signalling pathways, whilst offering a tunable cost function which the user can adjust the characteristics of an 'optimal' response. The controller can be tuned to focus on: the duration of the output state errors; how quickly the inputs change; and the use of the inputs themselves. The weights can also be changed during its operation to choose different drug profiles that will achieve a similar performance whilst giving the cell a break from individual drugs to slow the process of resistance. In the future we hope to test the controller on a microfuidics device as currently the controller has only been tested *in-silico*.

References

[1] M. Khammash, M. Di Bernardo, and D. Di Bernardo. Cybergenetics: Theory and Methods for Genetic Control System. *Proceedings of the IEEE Conference on Decision and Control*, 2019-December:916–926, 12 2019. doi:10.1109/CDC40024.2019.9030209.

[2] Elisa Pedone et al. A tunable dual-input system for on-demand dynamic gene expression regulation. *Nature communications*, 2019. doi:10.1038/s41467-019-12329-9.

[3] Ciarán Ciar´, Ciarán L Kelly, Andreas W K Harris, Harrison Steel, Edward J Hancock, John T Heap, and Antonis Papachristodoulou. Synthetic negative feedback circuits using engineered small RNAs. *Nucleic Acids Research*, 46(18):9875–9889, 2018. URL: https://academic.oup.com/nar/article/46/18/9875/5096075, doi:10.1093/nar/gky828.

[4] Stephanie K. Aoki, Gabriele Lillacci, Ankit Gupta, Armin Baumschlager, David Schweingruber, and Mustafa Khammash. A universal biomolecular integral feedback controller for robust perfect adaptation. *Nature 2019 570:7762*, 570(7762):533–537, 6 2019. URL: https://www.nature.com/articles/s41586-019-1321-1, doi:10.1038/s41586-019-1321-1.

[5] Victoria Hsiao, Emmanuel L.C. De Los Santos, Weston R. Whitaker, John E. Dueber, and Richard M. Murray. Design and implementation of a biomolecular concentration tracker. *ACS Synthetic Biology*, 4(2):150–161, 2 2015. URL: https://pubs.acs.org/doi/full/10.1021/sb500024b, doi:10.1021/SB500024B/SUPPL{_}FILE/SB500024B{_}SI{_}003.ZIP.

[6] Ryan J. Bloom, Sally M. Winkler, and Christina D. Smolke. Synthetic feedback control using an RNAi-based gene-regulatory device. *Journal of Biological Engineering*, 9(1):1–13, 4 2015. URL: https://jbioleng.biomedcentral.com/articles/10.1186/s13036-015-0002-3, doi:10.1186/S13036-015-0002-3/FIGURES/5.

[7] F Menolascina, G ¤ Fiore, E Orabona, De Stefano, and L Ferry. In-Vivo Real-Time Control of Protein Expression from Endogenous and Synthetic Gene Networks. *PLoS Comput Biol*, 10(5):1003625, 2014. URL: www.ploscompbiol.org, doi:10.1371/journal.pcbi.1003625.

[8] Andreas Milias-Argeitis, Sean Summers, Jacob Stewart-Ornstein, Ignacio Zuleta, David Pincus, Hana El-Samad, Mustafa Khammash, and John Lygeros. In silico feedback for in vivo regulation of a gene expression circuit. *Nature Biotechnology 2011 29:12*, 29(12):1114–1116, 11 2011. URL: https://www.nature.com/articles/nbt.2018, doi:10.1038/nbt.2018.

[9] Lorena Postiglione et al. Regulation of Gene Expression and Signaling Pathway Activity in Mammalian Cells by Automated Microfluidics Feedback Control. *ACS Synthetic Biology*, 7(11):2558–2565, 11 2018. URL: https://

pubs.acs.org/doi/pdf/10.1021/acssynbio.8b00235, doi:10.1021/ACSSYNBIO.8B00235/SUPPL{_}FILE/SB8B00235{_}SI{_}012.AVI.

[10] Jared E. Toettcher et al. Light-based feedback for controlling intracellular signaling dynamics. *Nature methods*, 8(10):837, 10 2011. URL: /pmc/articles/PMC3184382//pmc/articles/PMC3184382/?report=abstracthttps://www.ncbi.nlm.nih.gov/pmc/articles/PMC3184382/, doi:10.1038/NMETH.1700.

[11] Jannis Uhlendorf, Agnès Miermont, Thierry Delaveau, Gilles Charvin, François Fages, Samuel Bottani, Gregory Batt, Pascal Hersen, and David A Weitz. Long-term model predictive control of gene expression at the population and single-cell levels. *SYSTEMS BIOLOGY*, 109(35):14271–14276, 2012. URL: www.pnas.org/lookup/suppl/doi:10.1073/pnas.1206810109/-/DCSupplemental.www.pnas.org/cgi/doi/10.1073/pnas.1206810109, doi:10.1073/pnas.1206810109.

[12] Barbara Shannon, Criseida G. Zamora-Chimal, Lorena Postiglione, Davide Salzano, Claire S. Grierson, Lucia Marucci, Nigel J. Savery, and Mario Di Bernardo. In Vivo Feedback Control of an Antithetic Molecular-Titration Motif in Escherichia coli Using Microfluidics. *ACS Synthetic Biology*, 9(10):2617–2624, 10 2020. URL: https://pubs.acs.org/doi/abs/10.1021/acssynbio.0c00105, doi:10.1021/ACSSYNBIO.0C00105/SUPPL{_}FILE/SB0C00105{_}SI{_}002.ZIP.

[13] Irene De Cesare, Criseida G. Zamora-Chimal, Lorena Postiglione, Mahmoud Khazim, Elisa Pedone, Barbara Shannon, Gianfranco Fiore, Giansimone Perrino, Sara Napolitano, Diego Di Bernardo, Nigel J. Savery, Claire Grierson, Mario Di Bernardo, and Lucia Marucci. ChipSeg: An Automatic Tool to Segment Bacterial and Mammalian Cells Cultured in Microfluidic Devices. *ACS Omega*, 6(4):2473–2476, 2 2021. URL: https://pubmed.ncbi.nlm.nih.gov/33553865/, doi:10.1021/ACSOMEGA.0C03906/SUPPL{_}FILE/AO0C03906{_}SI{_}001.PDF.

[14] Elisa Pedone, Irene De Cesare, Criseida G. Zamora-Chimal, David Haener, Lorena Postiglione, Antonella La Regina, Barbara Shannon, Nigel J. Savery, Claire S. Grierson, Mario Di Bernardo, Thomas E. Gorochowski, and Lucia Marucci. Cheetah: A Computational Toolkit for Cybergenetic Control. *ACS Synthetic Biology*, 10(5):979–989, 5 2021. URL: https://pubs.acs.org/doi/full/10.1021/acssynbio.0c00463, doi:10.1021/ACSSYNBIO.0C00463/SUPPL{_}FILE/SB0C00463{_}SI{_}005.MOV.

[15] Mahmoud Khazim, Elisa Pedone, Lorena Postiglione, Diego di Bernardo, and Lucia Marucci. A Microfluidic/Microscopy-Based Platform for on-Chip Controlled Gene Expression in Mammalian Cells. *Methods in molecular biology (Clifton, N.J.)*, 2229:205–219, 2021. URL: https://pubmed.ncbi.nlm.nih.gov/33405224/, doi:10.1007/978-1-0716-1032-9{_}10.

[16] Mahmoud Khazim et al. Towards automated control of embryonic stem cell pluripotency. *IFAC-PapersOnLine*, 52(26):82–87, 1 2019. doi:10.1016/J.IFACOL.2019.12.240.

[17] Nicolas Kylilis, Zoltan A. Tuza, Guy Bart Stan, and Karen M. Polizzi. Tools for engineering coordinated system behaviour in synthetic microbial consortia. *Nature Communications 2018 9:1*, 9(1):1–9, 7 2018. URL: https://www.nature.com/articles/s41467-018-05046-2, doi:10.1038/s41467-018-05046-2.

[18] Gianfranco Fiore, Antoni Matyjaszkiewicz, Fabio Annunziata, Claire Grierson, Nigel J. Savery, Lucia Marucci, and Mario Di Bernardo. In-Silico Analysis and Implementation of a Multicellular Feedback Control Strategy in a Synthetic Bacterial Consortium. *ACS Synthetic Biology*, 6(3):507–517, 3 2017. URL: https://pubs.acs.org/doi/abs/10.1021/acssynbio.6b00220, doi:10.1021/ACSSYNBIO.6B00220/SUPPL{_}FILE/SB6B00220{_}SI{_}006.MPG.

[19] L. Postiglione, J. Wan, M. DI Bernardo, and L. Marucci. A strategy for multicellular feedback control in mammalian cells. *2019 18th European Control Conference, ECC 2019*, pages 2669–2674, 6 2019. doi:10.23919/ECC.2019.8796200.

[20] Antoni Matyjaszkiewicz, Gianfranco Fiore, Fabio Annunziata, Claire S. Grierson, Nigel J. Savery, Lucia Marucci, and Mario Di Bernardo. BSim 2.0: An Advanced Agent-Based Cell Simulator. *ACS Synthetic Biology*, 6(10):1969–1972, 10 2017. URL: https://pubs.acs.org/doi/full/10.1021/acssynbio.7b00121, doi:10.1021/ACSSYNBIO.7B00121/SUPPL{_}FILE/SB7B00121{_}SI{_}001.PDF.

[21] Lucia Marucci. Nanog Dynamics in Mouse Embryonic Stem Cells: Results from Systems Biology Approaches. *Stem cells international*, 2017, 2017. URL: https://pubmed.ncbi.nlm.nih.gov/28684962/, doi:10.1155/2017/7160419.

[22] Lucia Marucci, Stefania Santini, Mario di Bernardo, and Diego di Bernardo. Derivation, identification and validation of a computational model of a novel synthetic regulatory network in yeast. *Journal of mathematical biology*, 62(5):685–706, 5 2011. URL: https://pubmed.ncbi.nlm.nih.gov/20549211/, doi:10.1007/S00285-010-0350-Z.

[23] Alexander P. Browning, David J. Warne, Kevin Burrage, Ruth E. Baker, and Matthew J. Simpson. Identifiability analysis for stochastic differential equation models in systems biology. *Journal of the Royal Society Interface*, 17(173), 12 2020. URL: https://royalsocietypublishing.org/doi/abs/10.1098/rsif.2020.0652, doi:10.1098/RSIF.2020.0652.

[24] Ravi Salgia and Prakash Kulkarni. The genetic/non-genetic duality of drug 'resistance' in cancer. *Trends in cancer*, 4(2):110, 2 2018. URL: /pmc/articles/PMC5822736//pmc/articles/PMC5822736/?report=abstracthttps://www.ncbi.nlm.nih.gov/pmc/articles/PMC5822736/, doi:10.1016/J.TRECAN.2018.01.001.

[25] Neil Vasan, José Baselga, and David M. Hyman. A view on drug resistance in cancer. *Nature 2019 575:7782*, 575(7782):299–309, 11 2019. URL: https://www.nature.com/articles/s41586-019-1730-1, doi:10.1038/s41586-019-1730-1.

[26] Fortunato Bianconi et al. Computational model of EGFR and IGF1R pathways in lung cancer: A Systems Biology approach for Translational Oncology. *Biotechnology Advances*, 30(1):142–153, 1 2012. doi:10.1016/J.BIOTECHADV.2011.05.010.

[27] James Blake Rawlings et al. *Model predictive control : theory, computation, and design*. Nob Hill Publishing, 2nd edition, 2020.

[28] Jorrit J. Hornberg et al. Control of MAPK signalling: from complexity to what really matters. *Oncogene*, 24(36):5533–5542, 8 2005. URL: https://pubmed.ncbi.nlm.nih.gov/16007170/, doi:10.1038/SJ.ONC.1208817.

[29] Gianfranco Fiore et al. In Vivo Real-Time Control of Gene Expression: A Comparative Analysis of Feedback Control Strategies in Yeast. *ACS Synthetic Biology*, 5(2):154–162, 2 2015. URL: https://pubs.acs.org/doi/abs/10.1021/acssynbio.5b00135, doi:10.1021/ACSSYNBIO.5B00135.

[30] Vahideh Vakil and Wade Trappe. Drug Combinations: Mathematical Modeling and Networking Methods. *Pharmaceutics*, 11(5), 5 2019. URL: https://pubmed.ncbi.nlm.nih.gov/31052580/, doi:10.3390/PHARMACEUTICS11050208.

[31] Eugene Demidenkoid and Todd W Miller. Statistical determination of synergy based on Bliss definition of drugs independence. *PLOS ONE*, 2019. doi:10.1371/journal.pone.0224137.

[32] Pedro Albertos and Iven Mareels. Feedback and Control for Everyone. *IEEE Control Systems*, 31(4):93–95, 2011. doi:10.1109/MCS.2011.941441.

[33] Domitilla Del Vecchio et al. Headline review Control theory meets synthetic biology. *Interface*, 2016. URL: http://dx.doi.org/10.1098/rsif.2016.0380orviahttp://rsif.royalsocietypublishing.org., doi:10.1098/rsif.2016.0380.

[34] Jean-Baptiste Lugagne et al. Balancing a genetic toggle switch by real-time feedback control and periodic forcing. *Nature Communications*, 2017. URL: www.nature.com/naturecommunications, doi:10.1038/s41467-017-01498-0.

[35] Davide Fiore, Agostino Guarino, and Mario Di Bernardo. Analysis and control of genetic toggle switches subject to periodic multi-input stimulation. Technical report.

[36] Agostino Guarino, Davide Fiore, and Mario di Bernardo. In-silico Feedback Control of a MIMO Synthetic Toggle Switch via Pulse-Width Modulation. 11 2018. URL: https://www.researchgate.net/publication/328998015_In-silico_Feedback_Control_of_a_MIMO_Synthetic_Toggle_Switch_via_Pulse-Width_Modulationhttp://dx.doi.org/10.23919/ECC.2019.8795642, doi:10.23919/ECC.2019.8795642.

[37] Giansimone Perrino, Cathal Wilson, Marco Santorelli, and Diego di Bernardo. Quantitative Characterization of α-Synuclein Aggregation in Living Cells through Automated Microfluidics Feedback Control. *Cell reports*, 27(3):916–927, 4 2019. URL: https://pubmed.ncbi.nlm.nih.gov/30995486/, doi:10.1016/J.CELREP.2019.03.081.

[38] PI3K Inhibitor Review. https://www.selleckchem.com/PI3K.html. URL: https://www.selleckchem.com/PI3K.html.

[39] You Tong Wu et al. Dual role of 3-methyladenine in modulation of autophagy via different temporal patterns of inhibition on class I and III phosphoinositide 3-kinase. *The Journal of biological chemistry*, 285(14):10850–10861, 4 2010. URL: https://pubmed.ncbi.nlm.nih.gov/20123989/, doi:10.1074/JBC.M109.080796.

[40] Akt Inhibitor Review. https://www.selleckchem.com/Akt.html. URL: https://www.selleckchem.com/Akt.html.

[41] Huahong Yang et al. Oridonin sensitizes cisplatin-induced apoptosis via AMPK/Akt/mTOR-dependent autophagosome accumulation in A549 cells. *Frontiers in Oncology*, 9(AUG):769, 2019. doi:10.3389/FONC.2019.00769/BIBTEX.

[42] MEK Inhibitor Review. https://www.selleckchem.com/MEK.html. URL: https://www.selleckchem.com/MEK.html.

[43] Erika Martinelli et al. Antitumor activity of pimasertib, a selective MEK 1/2 inhibitor, in combination with PI3K/mTOR inhibitors or with multi-targeted kinase inhibitors in pimasertib-resistant human lung and colorectal cancer cells. *International journal of cancer*, 133(9):2089–2101, 11 2013. URL: https://pubmed.ncbi.nlm.nih.gov/23629727/, doi:10.1002/IJC.28236.

S1 NSCLC Closed Loop Model

The model of the NSCLC is

$$\dot{\mathbf{x}} = f(\mathbf{x}, \mathbf{u}), \qquad \mathbf{y} = \mathbf{C}\mathbf{x} = [0,0,0,0,0,0,0,1,0,0,0,1,0,0,0,0,0,0,0,0,0]\mathbf{x} \tag{S1}$$

where the vector field $f(.,.)$ is detailed in (S2)-(S21), $\mathbf{x}$ is the state vector containing 21 molecule concentrations (Table S1), $\mathbf{u}$ is the input vector $\mathbf{u} = [I_1, I_2, I_3]^T$ (orange in (S2)-(S21)) and $\mathbf{y}$ is the vector of outputs $y_1 = pERK$ and $y_2 = pAkt$ (blue in (S2)-(S21)).

x_i	**Shorthand**	**Molecule**
x_1	pEGFR	Active epidermal growth factor receptor
x_2	DSOS	Deactive SOS
x_3	SOS	Son Of Sevenless, a Guanine nucleotide exchange factor
x_4	Raf	Raf kinase
x_5	pRas	Active Ras, a small GTPase
x_6	pMEK	Active Methyl ethyl ketone
x_7	ERK	Extracellular-signal-regulated kinase
x_8	pERK	Active ERK
x_9	pIGF1R	Active Insulin-like growth factor receptor
x_{10}	PI3K	Phosphoinositide 3-kinase
x_{11}	pPI3K	Active PI3K
x_{12}	pAkt	Active Akt
x_{13}	Akt	Set of three serine/threonine-specific protein kinases
x_{14}	PP2A	Protein phosphatase 2, Kinase inhibitor
x_{15}	Ras	A small GTPase
x_{16}	pRaf	Active Raf
x_{17}	MEK	Methyl Ethyl Ketone
x_{18}	RasGAP	GTP hydrolyser of Ras
x_{19}	ppRaf	Raf which has been phosphorylated twice
x_{20}	P90	Ribosomal S6 kinase
x_{21}	pP90	Active P90

Table S1

$$\frac{\mathrm{d}pEGFR}{\mathrm{d}t} = -kf_E pEGFR - k_{SOS:E} pEGFR \frac{DSOS}{KM_{SOS:E} + DSOS} - k_{PI3K:E} pEGFR \frac{PI3K}{KM_{PI3K:E} + PI3K} \tag{S2}$$

$$\frac{\mathrm{d}pIGF1R}{\mathrm{d}t} = -kf_I pIGF1R - k_{SOS:I} pIGF1R \frac{DSOS}{KM_{SOS:I} + DSOS} - k_{PI3K:I} pIGF1R \frac{PI3K}{KM_{PI3K:I} + PI3K} \tag{S3}$$

$$\frac{\mathrm{d}SOS}{\mathrm{d}t} = k_{SOS:E} pEGFR \frac{DSOS}{KM_{SOS:E}+DSOS} + k_{SOS:I} pIGF1R \frac{DSOS}{KM_{SOS:I}+DSOS} - k_{DSOS:P90} pP90Rsk \frac{SOS}{KM_{DSOS:P90}+SOS} - k_{Ras:SOS} SOS \frac{Ras}{KM_{Ras:SOS}+Ras} \tag{S4}$$

$$\frac{\mathrm{d}DSOS}{\mathrm{d}t} = k_{DSOS:pP90} pP90Rsk \frac{SOS}{KM_{DSOS:pP90}+SOS} - k_{SOS:E} pEGFR \frac{DSOS}{KM_{SOS:E}+DSOS} - k_{SOS:I} pIGF1R \frac{DSOS}{KM_{SOS:I}+DSOS} \tag{S5}$$

$$\frac{\mathrm{d}pRas}{\mathrm{d}t} = k_{Ras:SOS} SOS \frac{Ras}{KM_{Ras:SOS}+Ras} - k_{Ras:Gab} RasGAP \frac{pRas}{KM_{Ras:Gab}+pRas} - k_{PI3K:Ras} pRas \frac{PI3K}{KM_{PI3K:Ras}+PI3K} - k_{Raf:Ras} pRas \frac{Raf}{KM_{Raf:Ras}+Raf} \tag{S6}$$

$$\frac{\mathrm{d}Ras}{\mathrm{d}t} = k_{Ras:SOS} SOS \frac{Ras}{KM_{Ras:SOS}+Ras} + k_{Ras:Gab} RasGAP \frac{pRas}{KM_{Ras:Gab}+pRas} \tag{S7}$$

$$\frac{\mathrm{d}pRaf}{\mathrm{d}t} = k_{Raf:Ras} pRas \frac{Raf}{KM_{Raf:Ras}+Raf} - k_{Raf:ppRaf} ppRaf \frac{pRaf}{KM_{Raf:ppRaf}+pRaf} - k_{Raf:Akt} pAkt \frac{pRaf}{KM_{Raf:Akt}+pRaf} - k_{Raf:MEK} pRaf \frac{MEK}{KM_{Raf:MEK}+MEK} \tag{S8}$$

$$\frac{\mathrm{d}Raf}{\mathrm{d}t} = -k_{Raf:Ras} pRas \frac{Raf}{KM_{Raf:Ras}+Raf} + k_{Raf:ppRaf} ppRaf \frac{pRaf}{KM_{Raf:ppRaf}+pRaf} + k_{Raf:Akt} pAkt \frac{pRaf}{KM_{Raf:Akt}+pRaf} \tag{S9}$$

$$\frac{\mathrm{d}Raf}{\mathrm{d}t} = -k_{Raf:Ras} pRas \frac{Raf}{KM_{Raf:Ras}+Raf} + k_{Raf:ppRaf} ppRaf \frac{pRaf}{KM_{Raf:ppRaf}+pRaf} + k_{Raf:Akt} pAkt \frac{pRaf}{KM_{Raf:Akt}+pRaf} \tag{S10}$$

$$\frac{\mathrm{d}MEK}{\mathrm{d}t} = -k_{MEK:Raf} pRaf \frac{MEK}{KM_{MEK:Raf}+MEK} + k_{MEK:PP2A} PP2A \frac{pMEK}{KM_{MEK:PP2A}+pMEK} - kon_3 MEK \frac{I_3}{Km_3+I3} \tag{S11}$$

$$\frac{\mathrm{d}pMEK}{\mathrm{d}t} = k_{MEK:Raf} pRaf \frac{MEK}{KM_{MEK:Raf}+MEK} - k_{MEK:PP2A} PP2A \frac{pMEK}{KM_{MEK:PP2A}+pMEK} - k_{ERK:MEK} pMEK \frac{ERK}{KM_{ERK:MEK}+ERK} - kon_3 pMEK \frac{I_3}{Km_3+I3} \tag{S12}$$

$$\frac{\mathrm{d}pERK}{\mathrm{d}t} = k_{ERK:MEK} pMEK \frac{ERK}{KM_{ERK:MEK}+ERK} - k_{ERK:PP2A} PP2A \frac{pERK}{KM_{ERK:PP2A}+pERK} - k_{DSOS:ERK} pERK \frac{SOS}{KM_{DSOS:ERK}+SOS} - k_{E:ERK} pERK \frac{pEGFR}{KM_{EGFR:ERK}+pEGFR} \tag{S13}$$

$$\frac{\mathrm{d}ERK}{\mathrm{d}t} = -k_{ERK:MEK} pMEK \frac{ERK}{KM_{ERK:MEK}+ERK} + k_{ERK:PP2A} PP2A \frac{pERK}{KM_{ERK:PP2A}+pERK} \tag{S14}$$

$$\frac{\mathrm{d}pP90Rsk}{\mathrm{d}t} = k_{pP90:ERK} pERK \frac{P90Rsk}{KM_{pP90:ERK}+P90Rsk} - k_{DSOS:pP90} pP90Rsk \frac{SOS}{KM_{DSOS:pP90}+SOS} \tag{S15}$$

$$\frac{\mathrm{d}P90Rsk}{\mathrm{d}t} = kd_{pP90Rsk} - k_{pP90:ERK} pERK \frac{P90Rsk}{KM_{pP90:ERK}+P90Rsk} \tag{S16}$$

$$\frac{\mathrm{d}pPI3K}{\mathrm{d}t} = k_{PI3K:Ras} pRas \frac{PI3K}{KM_{PI3K:Ras}+PI3K} + k_{PI3K:I} pIGF1R \frac{PI3K}{KM_{PI3K:I}+PI3K} + k_{PI3K:E} pEGFR \frac{PI3K}{KM_{PI3K:E}+PI3K} - k_{Akt:PI3K} Akt \frac{pPI3K}{KM_{Akt:PI3K}+pPI3K} - kd_{PI3K} pPI3K - kon_1 pPI3K \frac{I_1}{Km_1+I1} \tag{S17}$$

$$\frac{\mathrm{d}PI3K}{\mathrm{d}t} = -k_{PI3K:Ras}pRas\frac{PI3K}{KM_{PI3K:Ras}+PI3K} - k_{PI3K:I}pIGF1R\frac{PI3K}{KM_{PI3K:I}+PI3K} - k_{PI3K:E}pEGFR\frac{PI3K}{KM_{PI3K:E}+PI3K} + kd_{PI3K}pPI3K - kon_1PI3K\frac{I_1}{Km_1+I1} \tag{S18}$$

$$\frac{\mathrm{d}pAkt}{\mathrm{d}t} = -k_{Raf:Akt}pAkt\frac{pRaf}{KM_{Raf:Akt}+pRaf} + k_{Akt:PI3K}Akt\frac{pPI3K}{KM_{Akt:PI3K}+pPI3K} - kon_2pAkt\frac{I_2}{Km_2+I2} \tag{S19}$$

$$\frac{\mathrm{d}Akt}{\mathrm{d}t} = -k_{Akt:PI3K}Akt\frac{pPI3K}{KM_{Akt:PI3K}+pPI3K} + kd_{Akt}pAkt - kon_2Akt\frac{I_2}{Km_2+I2} \tag{S20}$$

$$\frac{\mathrm{d}RasGAP}{\mathrm{d}t} = 0 \quad \frac{\mathrm{d}ppRaf}{\mathrm{d}t} = 0 \quad \frac{\mathrm{d}PP2A}{\mathrm{d}t} = 0 \tag{S21}$$

S1.1 Conservation Equations

Each molecule can either be active, $p(.)$, or inactive, but there is a constant concentration of that molecule within the model. Therefore this total, $(.)_T$, is used to define the conservation equations.

$$\begin{array}{lll} EGFR_T = pEGFR + EGFR & IGF1R_T = pIGF1R + IGF1R & SOS_T = SOS + DSOS \\ Ras_T = pRas + Ras & Raf_T = pRaf + Raf & MEK_T = pMEK + MEK \\ ERK_T = pERK + ERK & PI3K_T = pPI3K + PI3K & Akt_T = pAkt + Akt \end{array} \tag{S22}$$

S1.2 Initial Conditions

Mutations present in the NSCLC cell can lead to an over-expression of EGFR and IGFR which leads to the formation of a tumour. To differentiate a NSCLC cell from a Wild Type cell, different initial conditions for $pEGFR$ and $pIGF1R$ are taken [26]. This change in initial conditions affects the response of the system as shown in Figure 2. These initial conditions are used for all the simulations where the NSCLC cell is being controlled.

$$\begin{array}{lll} \text{NSCLC Cell:} & pEGFR_0 = 800'000\ \mu M & pIGF1R_0 = 400'000\ \mu M \\ \text{Wild Type Cell:} & pEGFR_0 = 8'000\ \mu M & pIGF1R_0 = 8'000\ \mu M \end{array} \tag{S23}$$

$$\begin{array}{llll} SOS_0 = 120'000\ \mu M & Ras_0 = 120'000\ \mu M & Raf_0 = 120'000\ \mu M & MEK_0 = 600'000\ \mu M \\ ERK_0 = 600'000\ \mu M & P90Rsk_0 = 120'000\ \mu M & PI3K_0 = 120'000\ \mu M & ppRaf_0 = 120'000\ \mu M \\ & PP2A_0 = 120'000\ \mu M & RasGAP_0 = 120'000\ \mu M & \end{array} \tag{S24}$$

$$DSOS_0 = pRas_0 = pRaf_0 = pMEK_0 = pERK_0 = pP90Rsk_0 = pPI3K_0 = 0\ \mu M \tag{S25}$$

S1.3 Parameters

Variable	Definition	Value, [26]
kf_E	EGFR deactivation	0.02
$k_{SOS:E}$	Catalytic constant for SOS activation by EGFR	694.731
$KM_{SOS:E}$	Michaelis–Menten constant for SOS activation by EGFR	6086070.0
$k_{PI3K:E}$	Catalytic constant for PIK3 activation by EGFR	10.6737
$KM_{PI3K:E}$	Michaelis–Menten constant for PIK3 activation by EGFR	184912.0
kf_I	IGF1R deactivation	0.02
$k_{SOS:I}$	Catalytic constant for SOS activation by IGF1R	500.0
$KM_{SOS:I}$	Michaelis–Menten constant for SOS activation by IGF1R	1000000.0
$k_{PI3K:I}$	Catalytic constant for PIK3 activation by IGF1R	10.6737
$KM_{PI3K:I}$	Michaelis–Menten constant for PIK3 activation by IGF1R	184912.0
$k_{DSOS:P90}$	Catalytic constant for DSOS deactivation by p90Rsk	161197.0
$KM_{DSOS:P90}$	Michaelis–Menten constant for DSOS deactivation by p90Rsk	896896.0
$k_{Ras:SOS}$	Catalytic constant for Ras activation by SOS	32.344
$KM_{Ras:SOS}$	Michaelis–Menten constant for Ras activation by SOS	35954.3
$k_{Ras:Gab}$	Catalytic constant for Ras deactivation by RasGAP	1509.36
$KM_{Ras:Gab}$	Michaelis–Menten constant for Ras deactivation by RasGAP	1432410.0
$k_{Raf:Ras}$	Catalytic constant for Raf activation by Ras	0.884096
$KM_{Raf:Ras}$	Michaelis–Menten constant for Raf deactivation by Ras	62464.6
$k_{Raf:ppRaf}$	Catalytic constant for Raf deactivation by RafPP	0.126329
$KM_{Raf:ppRaf}$	Michaelis–Menten constant for Raf deactivation by RafPP	1061.71
$k_{Raf:Akt}$	Catalytic constant for Raf deactivation by Akt	15.1212
$KM_{Raf:Akt}$	Michaelis–Menten constant for Raf deactivation by Akt	119355.0
$k_{Raf:MEK}$	Catalytic constant for MEK activation by Raf	185.759
$KM_{Raf:MEK}$	Michaelis–Menten constant for MEK activation by Raf	4768350.0
$k_{MEK:PP2A}$	Catalytic constant for MEK deactivation by PP2A	2.83243
$KM_{MEK:PP2A}$	Michaelis–Menten constant for MEK deactivation by PP2A	518753.0
$k_{ERK:MEK}$	Catalytic constant for ERK activation by MEK	9.85367
$KM_{ERK:MEK}$	Michaelis–Menten constant for ERK deactivation by MEK	1007340.0
$k_{ERK:PP2A}$	Catalytic constant for ERK activation by PP2A	9.85367
$KM_{ERK:PP2A}$	Michaelis–Menten constant for ERK deactivation by PP2A	1007340.0
kd_{P90}	p90Rsk deactivation	0.0050
$k_{P90:ERK}$	Catalytic constant for p90Rsk activation by Erk	0.0213697
$KM_{P90:ERK}$	Michaelis–Menten constant for p90Rsk activation by Erk	763523.0
$k_{Akt:PI3K}$	Catalytic constant for Akt activation by PIK3	0.0566279
$KM_{Akt:PI3K}$	Michaelis–Menten constant for Akt activation by PIK3	653951.01
kd_{Akt}	Akt deactivation	0.0050
kd_{PI3K}	PI3K deactivation	0.0050
	Value estimated in this report	
Kon_1	Catalytic constant for PI3K deactivation by I_1	0.1
Km_1	Michaelis-Menten constant for PI3K deactivation by I_1	60
Kon_2	Catalytic constant for Akt deactivation by I_2	0.01
Km_2	Michaelis-Menten constant for Akt deactivation by I_2	8.9
Kon_3	Catalytic constant for ERK deactivation by I_3	2
Km_3	Michaelis-Menten constant for ERK deactivation by I_3	2.5

Table S2: The Parameters used in the NSCLC model with the six input related parameters added as discussed.

S2 Menten Parameter Choice

The equation governing the inputs reaction with the target molecule is given by

$$\frac{\mathrm{d}Target}{\mathrm{d}t} = -Target\frac{KonI}{Km + I}, \tag{S26}$$

where the Menten parameter values associated with each input are listed in Table S3.

Drug	$Km/\mu M$	$Kon/\mu M s^{-1}$
I_1 - 3MA	60 [38]	0.1 [39]
I_2 - Oridonin	8.9 [40]	0.01 [41]
I_3 - Pimasetib	2 [42]	2.5 [43]

Table S3

Km is equivalent to the IC_{50} value of the inhibitor being used on each target and is a property of the drug. To make the response of the controller inputs less 'switch like', inhibitors with relatively large IC_{50} values have been chosen.

Kon has then been chosen by comparing the model of the drug to a western blot (shown in Figure S1). It has been shown that the parameters in Table S3 are within a suitable range and can therefore show the benefits of using an external feedback loop to guide treatments.

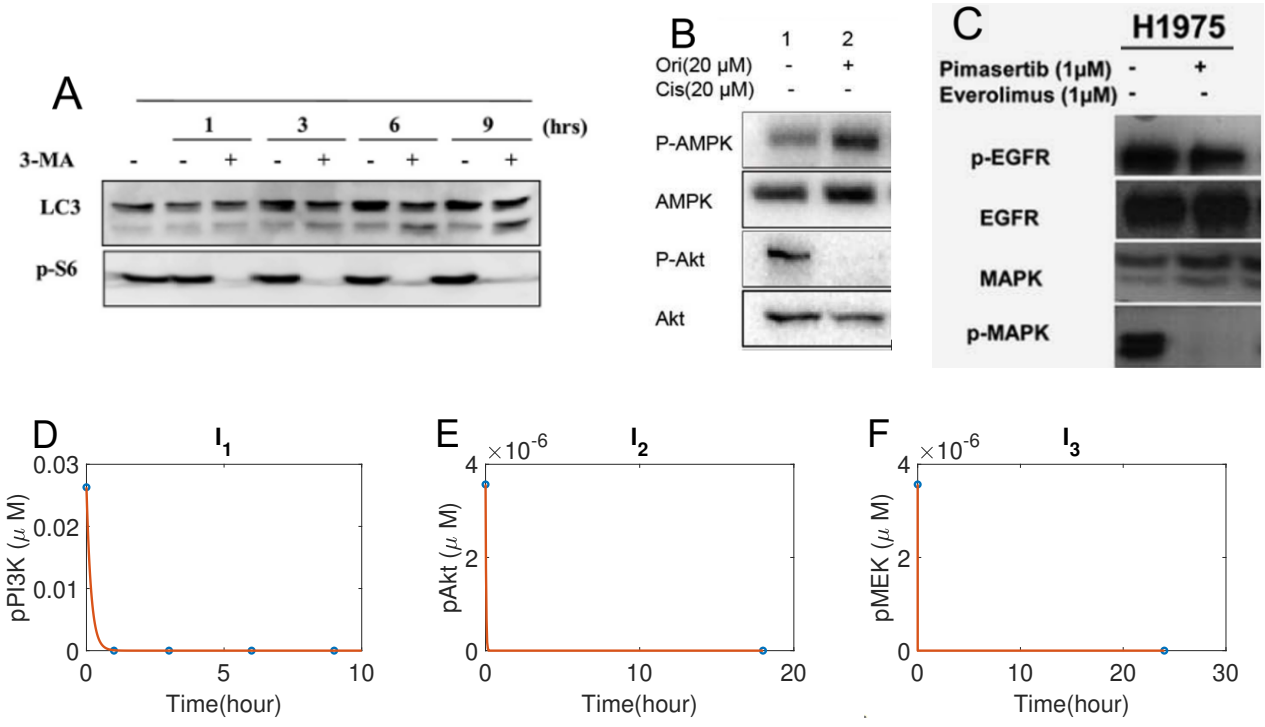

Figure S1: a)-c) Western Blot for 3MA [39], Ordonin [41] and Pimasetib [43], respectively. D)-f) A comparison of the western blot (circles) to the action of the Michaelis Menten term used to describe the 3MA [39], Ordonin [41] and Pimasetib [43], respectively. PI3K and MEK are unobservable therefore, p-S6 and pMAPK, respectively, have been used as markers for the related pathways.

Figure S2a shows the response of the system to step inputs I_1 (Figure S2b) for the Menten parameters Kon and Km used throughout the paper. The response of the system is highly sensitive to those parameters as they dictate how the input and NSCLC model interact. In particular, Kon controls the relative strength of the action of the inhibitor. If Kon is decreased by one order of magnitude, the step responses become almost identical to the system's free response (Figure S2C). Km dictates the 'switch like' behaviour of the inhibitor. For instance, if Km is decreased by an order of magnitude, the step response far overshoots the reference (Figure S2D). Increasing Km gives a similar effect as reducing Kon (not shown for conciseness).

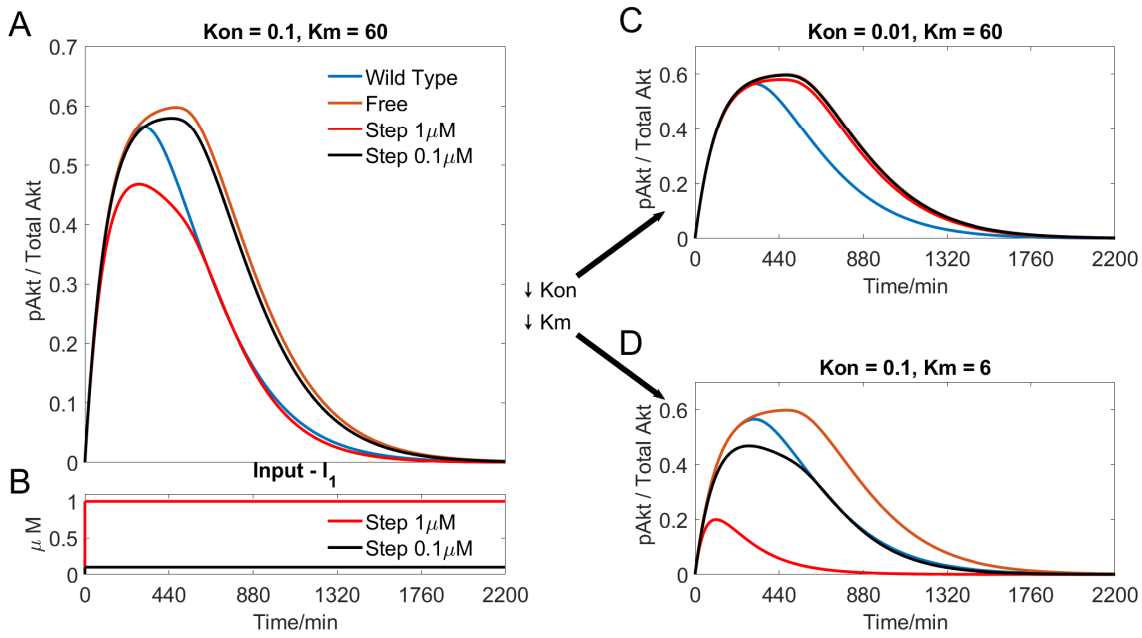

Figure S2: Step response simulations to show the affect of varied input parameters on the action of two different step inputs of I_1. A) Step response of Akt to the input parameters $Kon = 0.1$ and $Km = 60$, as used in subsequent simulations. B) The step inputs of I_1 used in the simulations. C) The step response of Akt if Kon had been reduced by a factor of ten ($Kon = 0.01$ and $Km = 60$). D) The step response of Akt if Km had been reduced by a factor of ten ($Kon = 0.1$ and $Km = 6$).

S3 Model Predictive Control (MPC)

MPC uses a model of the system in the feedback loop to predict how the system will behave in response to the inputs that the controller has optimally chosen at each time step. The inputs are chosen to minimise a user-defined cost function that typically includes terms penalising the magnitude of the inputs, $\mathbf{u}(t)$, and the magnitude of errors between the response of the system, $\mathbf{y}(t)$, and reference signals, $\mathbf{r}(t)$ [27]. For a given current state, MPC uses a model to show the dominant dynamics of the Plant to estimate the affect inputs would have on the actual plant. It then uses an optimiser to pick the 'optimal' input. The first set of 'optimal' inputs are then added to the system. The feedback loop then remeasure the outputs of the actual Plant to estimate the actual states and reiterates the MPC scheme to choose each subsequent input.

Some additions to the cost function will be discussed in Sections S3.2 and S3.3. MPC controllers are not limited to linear systems, however, non-linear systems will result in a larger computational effort and require more complex optimisation solvers, as discussed in Section S5.

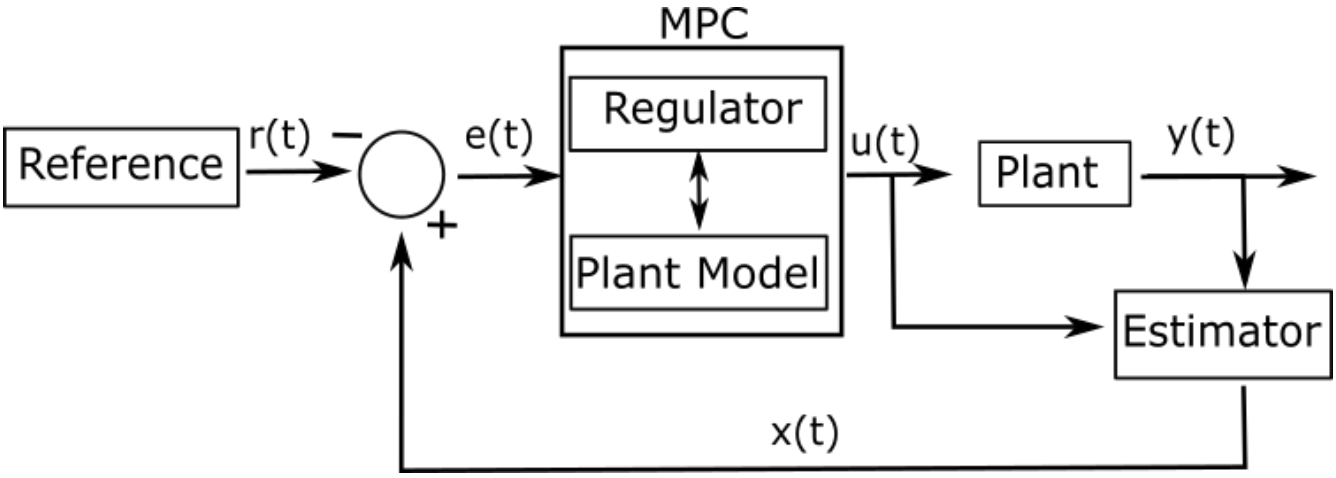

Figure S3: MPC scheme - a block diagram showing the flow of information around the control scheme, including what information is passed between each block

For the present numerical study, the plant is the nonlinear NSCLC model presented in Eqs. (S2)–(S21) and all the system states, $\mathbf{x}(t)$, are measured directly. In practice, only a few outputs/states can be measured and an estimator is required to estimate the remaining states from input-output data.

To sequester the downstream effect of the mutation within the cell, the control reference signal,$\mathbf{r}(t)$, is chosen as the response of the Wild type cell (i.e. without cancer). $\mathbf{e}(t)$ is the error signal between the reference, $\mathbf{r}(t)$, and internal states of the plant, $\mathbf{x}(t)$. $\mathbf{e}(t)$ is fed into the Regulation block of the control scheme, this is where the optimisation problem is solved, finding the minimum point of the cost function.

S3.1 Cost Function

Once the internal state errors, $\mathbf{e}(t)$, have been estimated or measured, the MPC controller can begin the optimally choose the input for the next time step. It does so by using the model of the system to predict the future state error of the system for all the possible combinations of inputs, within the problem constraints, over the prediction horizon. The controller then optimally chooses the input profile that results in the minimum of a predetermined cost function. The inputs of the first time step of the optimal input profile are then applied to the system. Therefore the MPC block contains the Plant Model, which is used to predict the future output of the system to various input profiles from the current state of the actual system, and the Regulator block, which receives these predictions and carries out the minimisation of the cost function to find the 'optimal' input.

Usually the optimisation problem contains the cost function, to be minimised, and the state and input con-

straints.

$$\min_{\mathbf{U}}(\mathbf{E}^T\mathbf{Q}\mathbf{E}+\mathbf{U}^T\mathbf{R}\mathbf{U}) \quad st. \quad -\mathbf{U}\leq\mathbf{U}_L, \quad \mathbf{U}\leq\mathbf{U}_U \tag{S27}$$

The model that the regulator sees is a discrete approximations of the NSCLC model for $1 \leq k \leq N$ steps. $\mathbf{E} = [\mathbf{e}(1), \mathbf{e}(2), \ldots, \mathbf{e}(N)]^T$ describing the current and future predicted state errors of the system. $\mathbf{U} = [\mathbf{u}(1), \mathbf{u}(2), \ldots, \mathbf{u}(N)]^T$ describes the future inputs. The proportion of the cost function related to each term can vary what is considered the 'optimal' input. $\mathbf{Q}$ weights the error of the states and $\mathbf{R}$ weights the use of the inputs. For example if the drugs used as an input need to be conserved then the weight of the cost function associated with the inputs, $\mathbf{R}$, should be relatively large compared to the weight of the state error, $\mathbf{Q}$. Affine constraints on the input bounds are also included here ($\mathbf{U}_L \leq \mathbf{U} \leq \mathbf{U}_U$, in all simulations $\mathbf{U}_L = 0\mu M$ and $\mathbf{U}_U = 1\mu M$) [27].

S3.1.1 Linear Model

If a linear approximation of the model can be produced and represented by a state space, the future behaviour of the model can be calculated offline and the optimisation problem is convex (for affine constraints). The minimal cost can then be solved using a quadratic solver, which is relatively computationally light (MATLAB's 'quadprog' solver has been used here).

It can be seen from Equation (S27) that the objective is to find the inputs to the system that minimize the cost function. As a discrete linear approximation of the model of the Plant can be used, a state space is used to represent the model, $\mathbf{e}(k+1) = \mathbf{A}\mathbf{e}(k) + \mathbf{B}\mathbf{u}(k)$, $\mathbf{y}(k) = \mathbf{C}\mathbf{e}(k) = g(\mathbf{e})$. Therefore as long as the current state is known, each future state can be estimated for a given input profile.

$$\begin{aligned}
\mathbf{e}(1) &= \mathbf{A}\mathbf{e}_0 + \mathbf{B}\mathbf{u}(1) \\
\mathbf{e}(2) &= \mathbf{A}\mathbf{e}_1 + \mathbf{B}\mathbf{u}(2) = \mathbf{A}(\mathbf{A}\mathbf{e}_0 + \mathbf{B}\mathbf{u}(1)) + \mathbf{B}\mathbf{u}(2) \\
\mathbf{e}(N) &= \mathbf{A}^N\mathbf{e}_0 + \mathbf{A}^{N-1}\mathbf{B}\mathbf{u}(1) + \mathbf{A}^{N-2}\mathbf{B}\mathbf{u}(2) + \ldots + \mathbf{B}\mathbf{u}(N)
\end{aligned} \tag{S28}$$

Defining a new notation containing all of the states in the prediction horizon.

$$\mathbf{E} = \mathbf{M}\mathbf{e}_0 + \tilde{\mathbf{C}}\mathbf{U}$$

$$\mathbf{U} = \begin{bmatrix} \mathbf{u}(1) \\ \mathbf{u}(2) \\ . \\ . \\ . \\ \mathbf{u}(N) \end{bmatrix} \quad \mathbf{M} = \begin{bmatrix} \mathbf{I} \\ \mathbf{A} \\ . \\ . \\ . \\ \mathbf{A}^N \end{bmatrix} \quad \tilde{\mathbf{C}} = \begin{bmatrix} \mathbf{0} & \mathbf{0} & . & . & . & \mathbf{0} \\ \mathbf{B} & \mathbf{0} & . & . & . & \mathbf{0} \\ \mathbf{AB} & \mathbf{B} & . & . & . & \mathbf{0} \\ . & & & & & \\ . & & & & & \\ \mathbf{A}^{N-1}\mathbf{B} & \mathbf{A}^{N-2}\mathbf{B} & . & . & . & \mathbf{B} \end{bmatrix} \tag{S29}$$

Therefore the cost function can be rearranged as

$$\begin{aligned} J(\mathbf{E},\mathbf{U}) &= \mathbf{E}^T\mathbf{Q}\mathbf{E} + \mathbf{U}^T\mathbf{R}\mathbf{U} \\ J(\mathbf{U}) &= (\mathbf{M}\mathbf{e}_0 + \tilde{\mathbf{C}}\mathbf{U})^T\mathbf{Q}(\mathbf{M}\mathbf{e}_0 + \tilde{\mathbf{C}}\mathbf{U}) + \mathbf{U}^T\mathbf{R}\mathbf{U} \\ &= \mathbf{U}^T(\tilde{\mathbf{C}}^T\mathbf{Q}\tilde{\mathbf{C}} + \mathbf{R})\mathbf{U} + 2\mathbf{e}_0^T(\tilde{\mathbf{C}}^T\mathbf{Q}\mathbf{M})^T\mathbf{U} + \mathbf{e}_0^T\mathbf{M}^T\mathbf{Q}\mathbf{M}\mathbf{e}_0 \\ &= \mathbf{U}^T\mathbf{H}\mathbf{U} + 2\mathbf{e}_0^T\mathbf{F}^T\mathbf{U} + \mathbf{e}_0^T\mathbf{G}\mathbf{e}_0 \end{aligned} \tag{S30}$$

The final term in the cost function can be removed as it is constant with respect to the inputs and therefore will not affect the position of the minimum points.

$$J(\mathbf{U}) = \mathbf{U}^T\mathbf{H}\mathbf{U} + 2\mathbf{e}_0^T\mathbf{F}^T\mathbf{U} \tag{S31}$$

Only the 'optimal' inputs for the first time step are then applied to the Plant, $\mathbf{u}(1)$, the whole optimization process is repeated at the next time step.

S3.1.2 Weighting

The cost function as shown in (S30), can be weighted as a balance of using the inputs, γ; the error in all of the estimated states, α and the error in the outputs, β.

$$\begin{aligned} \mathbf{Q} &= \alpha\mathbf{I} + \beta\begin{bmatrix} \mathbf{C}^T\mathbf{C} & \mathbf{0} & \dots & \mathbf{0} \\ \mathbf{0} & \mathbf{C}^T\mathbf{C} & \dots & \mathbf{0} \\ \mathbf{0} & \mathbf{0} & \dots & \mathbf{C}^T\mathbf{C} \end{bmatrix} \\ \mathbf{R} &= \begin{bmatrix} \gamma\mathbf{I} & \mathbf{0} & \dots & \mathbf{0} \\ \mathbf{0} & \gamma\mathbf{I} & \dots & \mathbf{0} \\ \mathbf{0} & \mathbf{0} & \dots & \gamma\mathbf{I} \end{bmatrix} \end{aligned} \tag{S32}$$

Where $\mathbf{C}$ from the state space approximation of the model and $\mathbf{I}$, a square identity matrix.

S3.2 Differential Input

The controller favoured jumping rapidly between input concentrations which is not be an 'optimal' input *in-vitro*. Therefore a term related to the gradient of the inputs is added to the cost function which works to reduce the fast variations of the input. The linear approximation of the model used within the MPC simulations is discrete and therefore the derivative is approximated by the scaled difference between each input at adjacent steps.

$$\frac{\mathrm{d}\mathbf{U}}{\mathrm{d}t}\Big|_k \approx \frac{\mathbf{U}(k) - \mathbf{U}(k-1)}{Ts} \tag{S33}$$

The terms that are independent of the inputs can be dropped from the cost function as they will only affect the value of the cost function but not its position. Similarly any constant scaling can be dropped as this would just

change the weighting added to the term. Using the squared sum of the derivative of the inputs, the gradient of the steps between the last actual input and the last step in the prediction horizon can be added to the cost function.

$$\begin{aligned}
&\textstyle\sum_{k=j}^{k=j+N}(\mathbf{U}(k)-\mathbf{U}(k-1))^2 = \sum_{k=j}^{k=j+N}\mathbf{U}(k)^2+\mathbf{U}(k-1)^2-2\mathbf{U}(k)\mathbf{U}(k-1)\\
&=\mathbf{U}(j-1)^2-2\mathbf{U}(j)\mathbf{U}(j-1)+2[\mathbf{U}(j)^2+\mathbf{U}(j+1)^2+\ldots+\mathbf{U}(j+N-1)^2\\
&\quad-\mathbf{U}(j)\mathbf{U}(j+1)-\mathbf{U}(j-1)\mathbf{U}(j-2)-\ldots-\mathbf{U}(j+N-1)\mathbf{U}(j+N)]+\mathbf{U}(j+N)^2\\
&=\mathbf{U}^T\mathbf{D}\mathbf{U}+\mathbf{d}\mathbf{U}\\
&\mathbf{D}=\theta\begin{bmatrix}2\mathbf{I}&-\mathbf{I}&\mathbf{0}&\ldots&\mathbf{0}\\-\mathbf{I}&2\mathbf{I}&-\mathbf{I}&\ldots&\mathbf{0}\\\mathbf{0}&-\mathbf{I}&2\mathbf{I}&\ldots&\mathbf{0}\\\vdots&\vdots&\vdots&\ddots&\vdots\\\mathbf{0}&\mathbf{0}&\mathbf{0}&\ldots&\mathbf{I}\end{bmatrix}\quad\mathbf{d}=\theta\begin{bmatrix}2\mathbf{U}(j-1)&\mathbf{0}&\mathbf{0}&\ldots&\mathbf{0}\end{bmatrix}
\end{aligned}\tag{S34}$$

Where $\mathbf{I}$ is a square identity matrix the size of the number of inputs. The gradient can be added to the cost function, J, through grouping the quadratic and proportional terms of the input's gradients and pre-multiplying by a scaling factor, θ.

$$\begin{aligned}
J(\mathbf{e}_0,\mathbf{U})&=\mathbf{U}^T\mathbf{H}\mathbf{U}+2\mathbf{e}_0^T\mathbf{F}^T\mathbf{U}+\mathbf{U}^T\mathbf{D}\mathbf{U}+\mathbf{d}\mathbf{U}\\
&=\mathbf{U}^T(\mathbf{H}+\mathbf{D})\mathbf{U}+(2\mathbf{e}_0^T\mathbf{F}^T+\mathbf{d})\mathbf{U}
\end{aligned}\tag{S35}$$

Figure 3, comparing plots C) and D) demonstrate the affect of the differential cost on preventing the rapidly changing inputs.

An alternative approach could be to add the gradient as a constraint into the optimisation problem, to physically prevent the inputs from varying faster than a limiting value. However, this does not inform the controller that the 'optimal' input should have slower changing inputs, it merely limits the maximum rate of variations.

S3.3 Integral State Error

When controlling the affect of signalling phosphorylation cascades, it is optimal to decrease both the peak and the duration of a molecule concentration higher up the cascade, rather than just its peak [28]. Both the duration and the peak are included in the integral of the error signal. Therefore the integral of the state errors should be added as a term in the cost function. The square of the integral errors has been approximated as shown.

$$
\begin{aligned}
\Big(\int_j^{j+N} \mathbf{e}(t)dt\Big)^2 &\approx \sum_{k=j}^{k=j+N} \mathbf{e}(k)^2 + \mathbf{e}(k-1)^2 + 2\mathbf{e}(k)\mathbf{e}(k-1) \\
&\approx \mathbf{e}(j-1)^2 + 2\mathbf{e}(j-1)\mathbf{e}(j) + \mathbf{e}(j+N)^2 + \\
&\quad 2\Big(\mathbf{e}(j)^2 + \ldots + \mathbf{e}(j+N-1)^2 + \mathbf{e}(j)\mathbf{e}(j+1) + \mathbf{e}(j+1)\mathbf{e}(j+2) + \ldots + \mathbf{e}(j+N-1)\mathbf{e}(j+N)\Big) \\
&\approx \mathbf{E}^T\mathbf{P}\mathbf{E} + \mathbf{p}\mathbf{E} \\
\mathbf{P} = \eta \begin{bmatrix} 2\mathbf{C}^T\mathbf{C} & \mathbf{C}^T\mathbf{C} & \mathbf{0} & \ldots & \mathbf{0} \\ \mathbf{C}^T\mathbf{C} & 2\mathbf{C}^T\mathbf{C} & \mathbf{C}^T\mathbf{C} & \ldots & \mathbf{0} \\ \mathbf{0} & \mathbf{C}^T\mathbf{C} & 2\mathbf{C}^T\mathbf{C} & \ldots & \mathbf{0} \\ \vdots & \vdots & \vdots & \ddots & \vdots \\ \mathbf{0} & \mathbf{0} & \mathbf{0} & \ldots & \mathbf{C}^T\mathbf{C} \end{bmatrix} & \quad \mathbf{p} = \eta \begin{bmatrix} \mathbf{0} & 2\mathbf{e}_0^T & \mathbf{0} & \ldots & \mathbf{0} \end{bmatrix}
\end{aligned}
\tag{S36}
$$

The first term is constant and is therefore dropped. $\mathbf{P}$ and $\mathbf{p}$ are weighted by η in the cost function. The integral cost is in terms of the future state errors $\mathbf{E}$ rather than the inputs $\mathbf{U}$. The matrices defined in Equation (S29), can be used.

$$
\begin{aligned}
\mathbf{E}^T\mathbf{P}\mathbf{E} + \mathbf{p}\mathbf{E} &= (\mathbf{M}\mathbf{e}_0 + \tilde{\mathbf{C}}\mathbf{U})^T\mathbf{P}(\mathbf{M}\mathbf{e}_0 + \tilde{\mathbf{C}}\mathbf{U}) + \mathbf{p}(\mathbf{M}\mathbf{e}_0 + \tilde{\mathbf{C}}\mathbf{U}) \\
&= \mathbf{e}_0^T\mathbf{M}^T\mathbf{P}\mathbf{M}\mathbf{e}_0 + \mathbf{U}^T\tilde{\mathbf{C}}^T\mathbf{P}\tilde{\mathbf{C}}\mathbf{U} + 2\mathbf{e}_0^T\mathbf{M}^T\mathbf{P}\tilde{\mathbf{C}}\mathbf{U} + \mathbf{p}\mathbf{M}\mathbf{e}_0 + \mathbf{p}\tilde{\mathbf{C}}\mathbf{U}
\end{aligned}
\tag{S37}
$$

The constant terms with respect to $\mathbf{U}$ can be dropped and the quadratic and proportional terms reorganised.

$$
\begin{aligned}
\mathbf{U}^T\tilde{\mathbf{C}}^T\mathbf{P}\tilde{\mathbf{C}}\mathbf{U} + 2\mathbf{e}_0^T\mathbf{M}^T\mathbf{P}\tilde{\mathbf{C}}\mathbf{U} + \mathbf{p}\tilde{\mathbf{C}}\mathbf{U} &= \mathbf{U}^T\tilde{\mathbf{P}}\mathbf{U} + \tilde{\mathbf{p}}\mathbf{U} \\
\tilde{\mathbf{P}} = \tilde{\mathbf{C}}^T\mathbf{P}\tilde{\mathbf{C}} \quad \tilde{\mathbf{p}} &= \mathbf{p}\tilde{\mathbf{C}} + (2\mathbf{e}_0^T\mathbf{M}^T\mathbf{P}\tilde{\mathbf{C}})
\end{aligned}
\tag{S38}
$$

The cost function, $J(\mathbf{U})$, can be formed including the integral of the state error.

$$
\begin{aligned}
J(\mathbf{U}) &= \mathbf{U}^T\mathbf{H}\mathbf{U} + \mathbf{U}^T\mathbf{D}\mathbf{U} + \mathbf{U}^T\tilde{\mathbf{P}}\mathbf{U} + 2\mathbf{e}_0^T\mathbf{F}\mathbf{U} + \mathbf{d}\mathbf{U} + \tilde{\mathbf{p}}\mathbf{U} \\
&= \mathbf{U}^T(\mathbf{H} + \mathbf{D} + \tilde{\mathbf{P}})\mathbf{U} + (2\mathbf{e}_0^T\mathbf{F} + \mathbf{d} + \tilde{\mathbf{p}})\mathbf{U}
\end{aligned}
\tag{S39}
$$

This is the cost function that has been used in all the simulations. Figure 3a demonstrates the affect of the integral cost on reducing both the amplitude and the duration of the error signal.

S3.4 Adaptive MPC

Adaptive MPC is a broad term describing MPC control schemes in which the model of the Plant changes as the simulation progresses, as briefly described in Section 2.1.1. The adaptive linear MPC has a better performance than a single linear model and is less computationally expensive than using a full non-linear model. Our non-linear model of the NSCLC, (S2) - (S21), can be linearised about a point to produce a linear model which is accurate about a localised region. Therefore at each iteration of the MPC algorithm, (at each time step) the non-linear model can

be linearised about the estimate of the states of the actual Plant in order to produce a linear approximation of the NSCLC model that updated each time step to better represent the dynamics of the Plant. This linear approximation can be ran through the MPC algorithm to predict the future behaviour of the linear system, representing the local future behaviour of the non-linear system and therefore the Plant.

S3.5 Cross-talk

Within the NSCLC cell there are many signalling pathways which all interact with each other. These pathways will propagate the affect of the mutation throughout the cell and therefore have evolved to cumulatively work against the treatment in one pathway through increasing the activation of another. The affect of the crosstalk between the MAPK and mTOR pathways is small and will not significantly affect the MPC controller. However if we run a MISO simulation where the controller is only allowed to use I_1 and I_2 whilst observing the error in y1 - ERK, the controller pulses each input for two minutes at the start of the simulation and then does not act again. In this simulation, $EI = 2.4034$, where as the EI of a free response when no input is used is, $EI = 2.4002$, showing that with the crosstalk modelled here the inputs used on the mTOR pathway to reduce the activation of Akt will go on to increase the activation of ERK in the MAPK pathway, as expected, as the robust network of pathways is attempting to dampen the affect of the external input. Figure S5 shows the affect of this cross-talk on a step input of both I_1 and I_2, showing that an input that would reduce the activation of y2 - Akt, also causes an increase in the activation of y1 - ERK as a EI of $2.4237 > 2.4002$.

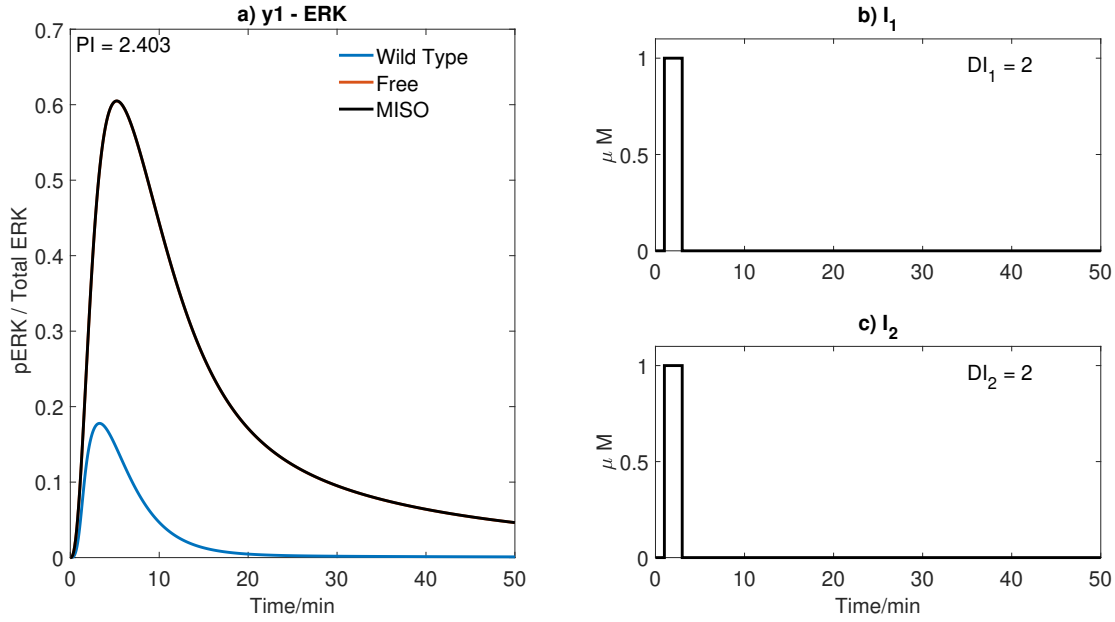

Figure S4: **I would not include this in the paper but just to show that the controller doesn't really act on the other pathway.**A MISO Linear MPC simulation using I_1 and I_2 to control the concentration of y1 - ERK. A) The response of ERK. B) and C) The inputs used in the simulation. Parameters: $T_s = 1min$, $N = 10$, $\alpha = 0$, $\beta = 0$, $\gamma = [1, 10^5, -]$, $\theta = 0$ and $\eta = 1$.

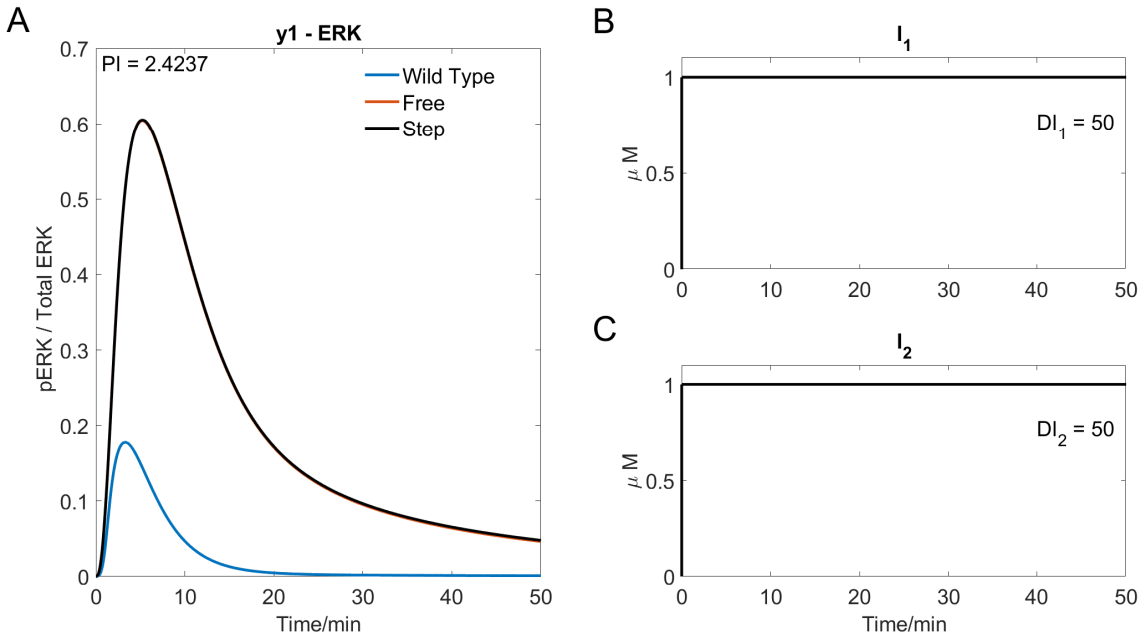

Figure S5: A step response simulation using I_1 and I_2. A) The response of ERK. B) and C) The step of 1 μM of I_1 and I_2 respectively.

S4 Indexes

In order to easily compare simulations it is useful to have an index to summarise the performance of the controller and the input it takes to achieve this performance, EI and DI_i respectively. These have been briefly defined in Section 2.1.3 and are normalised here such that multiple plots can be compared within Figure 7.

Firstly, the Error Index, EI, is the sum of the squared errors of the outputs, calculated by integrating the square of all the output error signals by using a trapezium approximation of the discrete data.

$$\begin{aligned} EI &= \int_0^T \mathbf{e}^T \mathbf{C} \mathbf{e}\, dt \\ \hat{EI} &= \frac{EI}{\max\limits_{\gamma_2/\gamma_1}(EI)} = \frac{EI}{EI_{I_1 SISO}} \end{aligned} \tag{S40}$$

All EIs have been divided by the lowest EI of any MISO simulation. It is expected that this would come at one of the SISO simulations ($R \to 0$ or $R \to \infty$) as using a combination of I_1 and I_2 should be better than either one by itself. The maximum EI found was the SISO simulation of I_1, therefore this has been used to normalise the EI to form $\hat{EI}$.

The dose of the inputs have to be non-negative and therefore the DI_i does not have to be squared. DI_i is equivalent to the integration of input profile for each input, i.

$$\begin{aligned} DI_i &= \int_0^T I_i(t)\, dt, \quad DI_{iSISO} = \int_0^T I_i^{SISO}(t)\, dt \\ \hat{DI}_i &= \frac{DI_i}{DI_{iSISO}} \end{aligned} \tag{S41}$$

It is expected that the largest dose of any one input would occur in the SISO simulation where it is the only input acting on the system. This was found to be true and DI_i is normalised by the DI_i of their own SISO simulation, producing $\hat{DI}_i$.

$\hat{DI}_i$ does not give a quantitative measure on the dose of the combined input profile. Within current literature, there are many methods of trying to summarises the joint affect and toxicity of static dosages of combined therapies [30], however these do not look into dynamic dosages over a given time period. Therefore a combined affect of the drug profiles can be estimated by replacing these static drug dosages with the normalised Dose Index, $\hat{DI}_i$.

An Isobole can be defined as $Iso = \hat{DI}_1 + \hat{DI}_2$ for these therapies. From this definition our combinations are all antagonistic. The Bliss Independence formula, BI, assumes that there is no correlation between the two agents.

$$BI = \hat{DI}_1 + \hat{DI}_2 - \hat{DI}_1 \hat{DI}_2 \tag{S42}$$

Our model is deterministic, with each input having a different target molecule, therefore within these *in-silica* simulations there is no correlation between the inputs. Therefore the Bliss Independence formula can be used to gauge the combined affect of 2 drugs [31]. All three indexes are used in Figure 7 to compare multiple simulations.

S5 Linear vs Non-Linear MPC

All MPC simulations within the report use an adaptive linear MPC controller, where the linear model is based off a linearisation of a non-linear model of the NSCLC system (S2)-(S21). Using the non-linear model creates a non-convex optimisation problem requiring a more complex (and computationally heavy) solver, with no guarantee of finding the global minimum. Here the non-linear simulations have used MATLAB's 'fmincon', a gradient based non-linear solver. It is the fastest appropriate non-linear solver. Due to the large number of internal states in the non-linear NSCLC model, a solver would take longer to find a solution than the current time step of the controller.

Non-linear MPC would limit the controller's use *in-vitro*, as the it would take longer to process the observations than time between observations. Resulting in a large time step for the controller, which could miss key dynamics of the system, as can be seen by comparing the performance of Figure 5 to 6. However when using the adaptive linear MPC controller the simulation takes a few seconds (well within the time step) and can still summarises key dynamics of the system even though some of the non-linear couplings between the states will be lost.

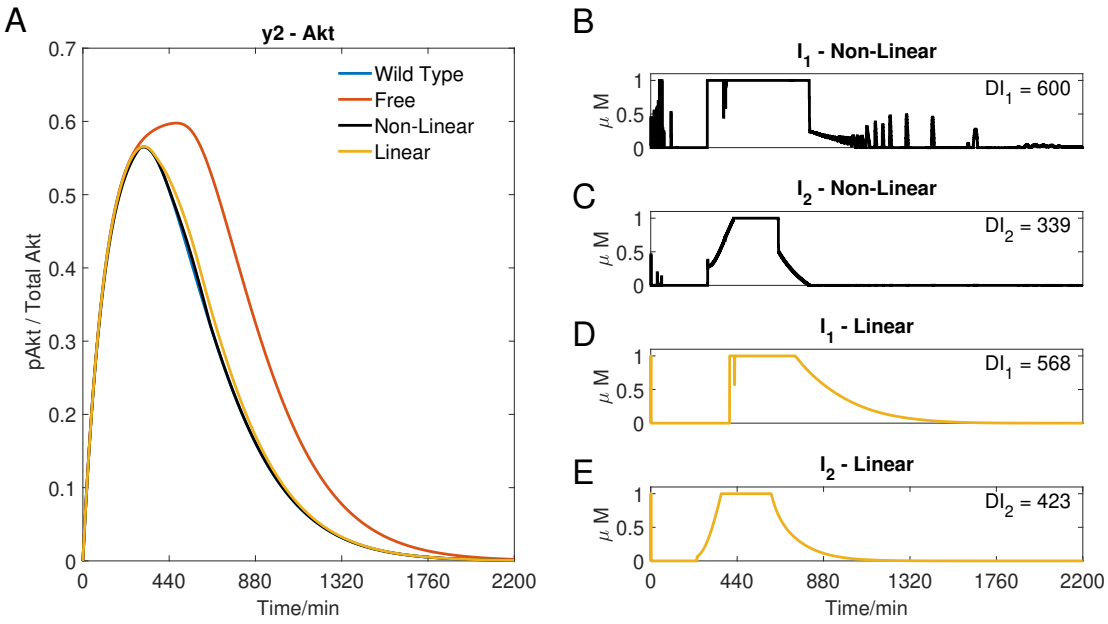

Figure S6: Two MPC simulations using I_1 and I_2 to control the concentration of y2 - Akt. A) the response of Akt to a non-linear MPC controller and an adaptive linear MPC controller. B) and C), the input of I_1 and I_2, respectively, used in the non-linear simulation. D) and E), the input of I_1 and I_2, respectively, used in the linear simulation. Parameters: $T_s = 1$, $N = 10$, $\alpha = 0$, $\beta = 0$, $\gamma = [1, 10^5, -]$, $\theta = 0$ and $\eta = 1$.

Figure S6 compares a MISO response using the adaptive linear MPC controller to a non-linear MPC controller. It can be seen that the non-linear MPC has a lower Error Index, however the run-time for the non-linear MPC simulation is 91'000 seconds, whereas the adaptive linear MPC has a run-time of only 33 seconds. The non-linear MPC has a significantly higher run-time, as expected.

S6 MPC vs PID

All feedback simulations within the report use an adaptive MPC controller. Figure S7 compares the performance of a feedback loop containing an MPC controller to one containing a simpler PID controller. Due to the relatively slow acting input, as observed in the outputs, a differential gain is not required in the PID controller. If an integral gain is added then the inputs have a non-zero steady state response, causing a very high DI. This is due to the fact that there is no integral anti wind up term in the controller and therefore the integral error never resets to zero, leaving the inputs at a non-zero state. Therefore a Proportional controller has been used.

Through simulations these two gains (a proportional gain for each input) can be tuned such that the controllers initial reaction to the error signal results in a relatively low EI, as shown in Figure S7, however the response is very sensitive to the choice of these gains. It can be seen in plots B) and C) that the inputs are identical, as the controller has no idea what is going on in the system that it is controlling.

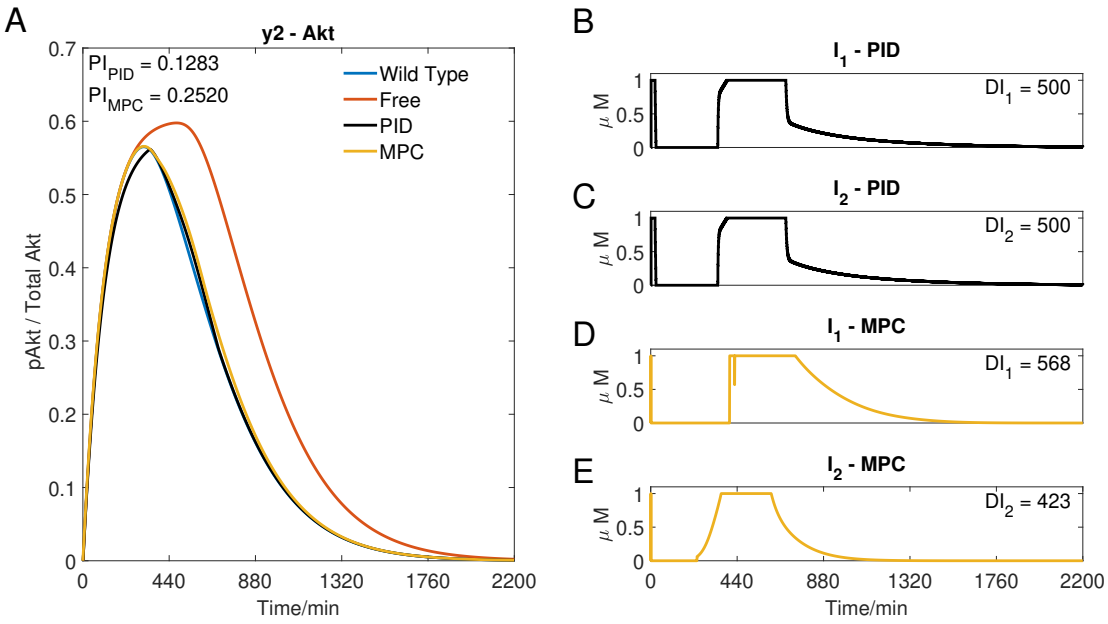

Figure S7: A comparison of a PID and MPC controllers used in the feedback loop using I_1 and I_2 to control the concentration of y2 - Akt. A) the response of Akt to a Proportional controller and an adaptive linear MPC controller. B) and C), the input of I_1 and I_2, respectively, used in the PID simulation. The proportional gains $Kp_{I_1} = 0.001$ and $Kp_{I_2} = 0.001$. D) and E), the input of I_1 and I_2, respectively, used in the MPC simulation. Parameters: $T_s = 1$, $N = 10$, $\alpha = 0$, $\beta = 0$, $\gamma = [1, 10^5, -]$, $\theta = 0$ and $\eta = 1$.

It can be seen that although the controllers result in a similar performance, the PID controller offers no control on the inputs used to get there and therefore would be of no use when trying to design different drug profiles that achieve a similar performance whilst not achieving robust control as the low EI is just as an effect of the finely tuned gains reacting to the measured initial error in the first two minutes. Whereas the MPC controller, through the cost function, can be told to priorities different input profiles.